INFORMATION TO USERS

This manuscript has been reproduced from the microfilm master. UMI films the text directly from the original or copy submitted. Thus, some thesis and dissertation copies are in typewriter face, while others may be from any type of computer printer.

The quality of this reproduction is dependent upon the quality of the copy submitted. Broken or indistinct print, colored or poor quality illustrations and photographs, print bleedthrough, substandard margins, and improper alignment can adversely affect reproduction.

In the unlikely event that the author did not send UMI a complete manuscript and there are missing pages, these will be noted. Also, if unauthorized copyright material had to be removed, a note will indicate the deletion.

Oversize materials (e.g., maps, drawings, charts) are reproduced by sectioning the original, beginning at the upper left-hand corner and continuing from left to right in equal sections with small overlaps. Each original is also photographed in one exposure and is included in reduced form at the back of the book.

Photographs included in the original manuscript have been reproduced xerographically in this copy. Higher quality 6" x 9" black and white photographic prints are available for any photographs or illustrations appearing in this copy for an additional charge. Contact UMI directly to order.

UMI

A Bell & Howell Information Company
300 North Zeeb Road, Ann Arbor, MI 48106-1346 USA
313/761-4700 800/521-0600

DYNAMICAL EQUILIBRATION OF A SPATIALLY PERIODIC FLOW OF CONDUCTING FLUID WITH AN EMBEDDED MAGNETIC FIELD: TOWARD A SELF-CONSISTENT ALPHA-SQUARED DYNAMO MODEL

A DISSERTATION SUBMITTED TO THE GRADUATE DIVISION OF
THE UNIVERSITY OF HAWAII IN PARTIAL FULFILLMENT
OF THE REQUIREMENTS FOR THE DEGREE OF

DOCTOR OF PHILOSOPHY
IN
GEOLOGY AND GEOPHYSICS

DECEMBER 1994

By

Jack Frederick McMillan

Dissertation Committee:
Augustine S. Furumoto, Chairman
Emilio Herrero-Bervera
Jonathan Gradie
David Bercovici
Arnold Feldman

UMI Number: 9519466

UMI Microform 9519466
Copyright 1995, by UMI Company. All rights reserved.

This microform edition is protected against unauthorized
copying under Title 17, United States Code.

UMI

300 North Zeeb Road
Ann Arbor, MI 48103

C COPYRIGHT 1994

Jack F. McMillan

Abstract

Spatially periodic flows possessing helicity exhibit dynamo action. One such flow studied by G.O. Roberts serves as the model in this thesis. The first results detail the structure of the flow, including its symmetry properties as ascertained by group-theoretical methods. A kinematic dynamo model at low magnetic Reynolds number is developed in the third chapter. It is found that magnetic fields with axial wavenumbers $O(R_M^2)$ are destabilised by the fluid motions, producing a dynamo effect. Roberts' cellular flow is next utilised to develop a simplified self-consistent dynamo model. The Navier-Stokes and induction equations are integrated over a cellular region in the $x-y$ plane. Degrees of freedom are recovered by imposing time-dependent amplitudes on the axial and planar velocities. The resulting set of three scalar evolution equations for the mean magnetic field energy density and velocity amplitudes are made nondimensional. The model thus represents a hydromagnetic analogue of the disc dynamo problem. Equilibria of the three variables are determined in terms of four dimensionless parameters arising from the analysis. The bifurcation structure of the system is analyzed, leading to a minimal criterion for dynamo action. Using linear stability analysis, mean magnetic field growth rates are determined in the regimes of the parameter space specified by the bifurcations. In a concluding chapter, implications for the geodynamo are discussed.

Contents

Abstract iv

List of Tables viii

List of Figures ix

1 GENERAL INTRODUCTION 1

1.1 Historical background 1

1.2 The dynamo problem 2

1.2.1 The induction equation 2

1.2.2 The infinite conductivity limit 4

1.2.3 The alpha effect 5

1.2.4 Time-scale for flux expulsion 7

1.2.5 Self-consistent dynamos 7

1.2.6 Types of dynamo models 8

1.3 Outline of the text 9

2 CHARACTERISTICS OF ROBERTS CELL MOTION 12

2.1 Introduction 12

2.2 Prelimanary formalism 12

2.3 Development of the model flow 14

2.3.1 Stream function and velocity field 14

2.3.2 Vorticity and helical structure 15

2.3.3 Turnover time and Lagrangian motion 17

2.4 Flows and symmetries 19
2.4.1 Group properties of the flow 19
2.5 Chapter summary 24

3 LOW R_m INDUCTION IN THE MODEL FLOW 29
3.1 Chapter overview 29
3.2 First order smoothing at low R_m 29
3.2.1 Preliminary considerations 29
3.2.2 Calculation of the R_m order field 33
3.2.3 Higher order field terms 34
3.3 A mean field dynamo model 35
3.4 Chapter summary 36

4 DYNAMICAL BEHAVIOR AT LARGE R_m IN THE MODEL FLOW 37
4.1 Overview of the chapter 37
4.2 Previous results 38
4.2.1 Boundary layer analysis 38
4.3 Formulation of the mean field induction equation 39
4.4 The Axial momentum equation 40
4.5 The axial torque equation 42
4.6 Nondimensionalization of the equations 44

5 ANALYSIS OF THE DYNAMO EQUATIONS 47
5.1 Chapter overview 47
5.2 Equilibrium solutions of the model 47
5.2.1 Case of zero Z_e 48
5.2.2 Case of nonzero Z_e 48
5.2.3 Some special cases 49

5.3 Bifurcation structure of the Z_e values 49
5.4 Stabilty of the equilibria 50
5.5 Numerical integration of the model equations 51
5.5.1 Case of $2\gamma\mu > \nu$ 51
5.5.2 Case of $2\gamma\mu < \nu$ 51

6 SUMMARY OF THE MODEL 66

6.1 Analysis of the model 66
6.1.1 The model within the context of a rotating fluid 66
6.2 Stability and bifurcation analysis of the model 67
6.2.1 Magnetic stresses and pathlines 68
6.3 Future Directions 69
References 70

List of Tables

2.1 Group elements in D_4 20

2.2 Classes of the group D_4 21

2.3 Irreducible representations of the group elements 22

2.4 Character table for D_4 23

2.5 Transformation table 23

List of Figures

2.1 The Kolmogorov flow streamlines 25

2.2 Typical pathlines in the Roberts cell flow 26

2.3 Dependency of the turnover time on the stream function 27

2.4 Position versus time along a typical streamline 28

5.1 Stability diagram of Z_e 53

5.2 Bifurcation diagram of Z_e 54

5.3 Supercritical case: phase diagram of Z vs U. 55

5.4 Supercritical case: Z vs t. 56

5.5 Supercritical case: U vs t. 57

5.6 A decaying field. 58

5.7 Subcritical lower branch: a field decay 59

5.8 Subcritical branch: stability of upper branch. 60

5.9 Hopf bifurcation: V vs t. 61

5.10 Post-Hopf: U vs t. 62

5.11 Post Hopf: V vs t. 63

5.12 Post Hopf: Z vs t. 64

5.13 Post Hopf: Limit cycle. 65

Chapter 1

GENERAL INTRODUCTION

1.1 Historical background

Geomagnetic measurements were conducted in China and Europe centuries ago. By 1600 Sir William Gilbert had displayed the essentially dipolar nature of the earth's magnetic field (Furumoto, unpublished notes). Yet the idea of a fluid dynamo maintaining an embedded magnetic field only arose within this century when in 1919 Larmor posited cyclonic motions as the source of the intense fields associated with sunspots (Parker, 1979). His view of a sunspot as a storm was incorrect, yet the connection between magnetic fields and turbulent fluid motions provided the impetus for modern dynamo theory.

In 1934 Cowling produced the first anti-dynamo theorem which stated that axisymmetric fields cannot be maintained by purely axisymmetric motions. This developement posed theoretical difficulties as the nearly spherical symmetry of the planets and Sun made axisymmetric fluid motions appealing. Later, Zeldovich showed that purely planar motions are likewise incapable of maintaining an embedded magnetic field against Ohmic dissipation. Theorists then postulated that the class of admissible flows for dynamo action must be three-dimensional motions with nontrivial topologies (Parker, 1979).

Parker (1955) showed that small-scale helical motions can give rise to dynamo

action by generating a current flux parallel to the mean magnetic field. Steenbeck, Raedler, and Krause (1966) elaborated the mean-field electrodynamics, thereby providing mathematical rigor to Parker's heuristic model. They named the process envisaged by Parker the alpha effect. The influence of localized motions on large-scale magnetism was then firmly established.

Helical flows have received attention as candidiates for dynamo action. Formally, helicity is the scalar product of the fluid velocity with its vorticity integrated over the fluid domain. Like disc dynamos, helical flows lack reflectional symmetry, a property which supports dynamo action (cf. Moffatt, 1978). Such flows were first studied by G.O. Roberts (1970, 1972) who showed that they mostly behave as first-order dynamos, i.e., the first perturbative term in the magnetic field modal expansion exhibits a positive growth rate.

A particular periodic flow that has received much attention is the Roberts cell, whose streamfunction is given by $\sin x \sin y$. Arising from the superposition of two helical waves, the flow consists of square cells reminiscent of patterns found in Rayleigh convection. Numerous studies of the Roberts cell as a kinematic dynamo have been made (Childress, 1979; Anufriyev and Fishman, 1982; Perkins and Zweibel, 1987) including the high conductivity limit (cf. Soward, 1987). Incorporation of dynamics into the cellular flow dynamo is developed in the present work.

1.2 The dynamo problem

1.2.1 The induction equation

If a magnetic field is embedded within an electrically conducting fluid, any motion of the fluid will generate currents due to the induced electric field. Magnetic energy is then dissipated through Joule heating. The currents also generate magnetic fields which can enhance the embedded magnetic field under certain flow topologies. Regeneration of magnetic field lines by fluid motions to counteract Ohmic decay

is the primary mechanism for the maintenance of magnetic fields in astrophysical bodies with fluid regions such as planets, stars, and even galaxies. The study of such processes constitute hydromagnetic dynamo theory.

The evolution of a magnetic field $\vec{b}$ in a fluid with velocity $\vec{u}$ is governed by the magnetohydrodynamic induction equation which is derivable from Maxwell's equations and Ohm's law,

$$\frac{\partial \vec{b}}{\partial t} = \nabla \times (\vec{u} \times \vec{b}) + \eta \nabla^2 \vec{b}. \tag{1.1}$$

The magnetic diffusivity $\eta = (\mu\sigma)^{-1}$ where σ is the conductivity and μ the permeability.

The dynamo problem consists of finding flows in which the nonmagnetic state is unstable (the dynamo instability) allowing for exponential growth of an initial seed field. Equation 1.1 is linear in $\vec{b}$ implying the field is determined only to within an arbitrary multiplicative constant. In kinematic dynamos, the magnetic amplitude is presumed small so that the velocity field remains unaltered. The Navier-Stokes equation may be then neglected.

For a steady flow $\vec{u} = \vec{u}(\vec{x})$, one can construct magnetic field representations of the form $\vec{b}(\vec{x}, t) = \vec{b}_p(\vec{x}) \exp pt$ (Childress and Ghil, 1986). It follows that the induction equation, with suitable boundary conditions, becomes an eigenvalue problem with the magnetic growth rate p being the eigenvalue:

$$p\ \vec{b}_p = \nabla \times \{\ \vec{u} \times \vec{b}_p\}) + \eta \nabla^2 \vec{b}_p. \tag{1.2}$$

Equation 1.2 constitutes a non-hermitian elliptic equation. The eigenvalue problem is well-posed if either Neumann or Dirichlet boundary conditions are imposed on $\vec{b}$ for a bounded flow (Barton, 1989). If the flow pervades all space, it is sufficient that the magnetic field be spatially periodic. Eigenvalues are discrete and generally complex with a point of accumulation at negative infinity. A dynamo exists when $Re\ (p) > 0$. Eigenfunctions may be countably degenerate (Bayley, private communi-

cation). An observation must be made here: the leading term (the Laplacian) in the differential operator on the right-hand side of (1.2) is hermitian. The non-hermitian advective term is of lower order as it involves only first derivatives and may be formally treated as a perturbation. Thus a complete eigenfunction basis set is constructible even though the operator is non-hermitian (Vishik, private communication). This is an important point, for without a complete basis set an eigenmodal expansion of the magnetic field would be of limited use (some magnetic states could then have a zero projection onto the eigenfunction set). Frequently in dynamo models growth rate become functions of the magnetic Reynolds number R_m which is the magnetic advection-diffusion ratio i.e., $R_m = \frac{|\nabla \times (\vec{u} \times \vec{b})|}{|\eta \nabla^2 \vec{b}|}$. The problem then becomes finding the critical magnetic Reynolds number for the onset of dynamo action.

1.2.2 The infinite conductivity limit

For a perfectly conducting fluid ($\sigma = \infty$), the diffusive term in the induction equation vanishes. This recasts the equation to read

$$\frac{\partial \vec{B}}{\partial t} = \nabla \times (\vec{u} \times \vec{B}), \tag{1.3}$$

where the Use of Lagrangian coordinates yields the Cauchy solution for the magnetic field's evolution. Density ρ appears due to mass continuity (cf. Moffatt, 1978).

$$\frac{B_i(\vec{x}, t)}{\rho(\vec{x}, t)} = \frac{\partial x_i}{\partial a_j} \frac{B_j(\vec{a}, 0)}{\rho(\vec{a}, 0)} \tag{1.4}$$

This result is a statment of the frozen flux theorem mentioned earlier. A particle initially at $\vec{a}$ remains on the same field line.

Diffusion in a stationary medium

A resistive fluid at rest provides the opposite case from above. Here $\vec{u} = 0$ and the induction equation reduces to a vector diffusion formula. Solving for $\vec{B}$ using the

heat equation Green's function in Cartesian coordinates yields for the magnetic field (Pearson, 1974; Parker, 1979)

$$\frac{\partial B_j}{\partial t} = \eta \nabla^2 B_j, \tag{1.5}$$

$$B_j(\vec{x},t) = (4\pi\eta t)^{-\frac{3}{2}} \int\int\int B_j(\vec{\xi},0) \exp\left\{-\frac{(\vec{x}-\vec{\xi})^2}{4\eta t}\right\} d^3\xi. \tag{1.6}$$

From (1.6) above, the field dissipates with a Gaussian profile. Large field gradients rapidly decay, while less sharply varying field lines smooth out more slowly. Diffusion of magnetic lines of force within a medium occurs on a timescale $t_d \sim \frac{L^2}{\eta}$ where L is a typical lengthscale of the system considered. For example, in the earth's core L may be taken as the radius R_{core}. The diffusion time is then $\sim 10^4$ years, which is consistent with current estimates of transition times at the onset of reversals.

1.2.3 The alpha effect

Parker (1955) envisaged a means to deform toroidal field lines into poloidal lines within a stellar convective zone. In his approach, a mass of rising fluid transports an embedded magnetic field. Stellar gases, being ionized, possess high electrical conductivities, so Alfven's theorem holds. The Coriolis force acts on the fluid mass causing it to spin. Such helical motions twist magnetic field lines into looplike configurations. Parker referred to this stretch-and-twist episode as a 'cyclonic event'. This process of field generation is called the alpha effect, named after the symbol used (Steenbeck, Rädler, and Krause 1966 ; Rädler and Krause, 1980). The alpha effect is due then to convection and rotation. An equivalent statement is that a toroidal current is generated parallel to the toroidal field thereby producing a poloidal field. This also was demonstrated in Parker's seminal paper (Parker, 1955b).

Mean-field magnetohydrodynamics (cf. Raedler and Krause, 1980) refers to a multi-scale method within dynamo theory. Specifically, one views the magnetic field as consisting of two parts: a mean field varying over large spatio-temporal scales and

a fluctuation from the mean, assumed to vary over smaller scales. In principle, the averaging method employed in determining the mean field may be spatial, temporal, or emsemble (Gibbs) averaging. The main criterion is that the two scales be widely separated, justifying the decomposition. One should not however assume the localized fluctuating field to be smaller in magnitude than the mean field; indeed within the solar convective zone, local field strengths of several thousand Gauss are achievable (based upon sunspot observations) while the large-scale solar field is only ~ 5 Gauss.

Assume the velocity and magnetic fields are divided in accordance with the mean-field hypothesis. Mean and fluctuating parts are given by

$$\vec{u}(\vec{x},t) \;=\; \vec{u}_0(\vec{x},t) \;+\; \vec{u}'(\vec{x},t), \tag{1.7}$$

$$\vec{b}(\vec{x},t) \;=\; \vec{b}_0(\vec{x},t) \;+\; \vec{b}'(\vec{x},t), \tag{1.8}$$

$$< \vec{u} > = \; \vec{u}_0, \; < \vec{u}' > = \; 0, \; < \vec{b} > = \; \vec{b}_0, \; < \vec{b}' > = \; 0. \tag{1.9}$$

In Eqs. 1.7-1.9, the averaging process is denoted by $< \cdot >$, averaged quantities have a '0' subscript and flucuating quantities are indicated by primes. Inserting the above expressions into the induction equation one obtains

$$\frac{\partial \vec{b}_0}{\partial t} \;=\; \nabla \times (\vec{u}_0 \times \vec{b}_0) \;+\; \nabla \times \vec{E}_0 \;+\; \eta \nabla^2 \vec{b}_0, \;\; \vec{E}_0 \;= < \vec{u} \times \vec{b} >, \tag{1.10}$$

$$\frac{\partial \vec{b}'}{\partial t} \;=\; \nabla \times (\vec{u}_0 \times \vec{b}' \;+\; \vec{u}' \times \vec{b}_0 \;+\; \vec{G}) \;+\; \eta \nabla^2 \vec{b}', \;\; \text{where } \vec{G} \;=\; \vec{u}' \times \vec{b}' \;-\; \vec{E}_0. \tag{1.11}$$

The mean electromotive force $\vec{E}_0$ acts as a source term in the mean-field induction equation and produces a mean current $\vec{J}_0 \;=\; \sigma \vec{E}_0$. In terms of the mean field $\vec{b}_0$ (Moffatt, 1978; Rädler and Krause, 1980).

$$E_i \;= \alpha_{ij} b_{0j} \;+\; \beta_{ijk} \frac{\partial b_{0j}}{\partial x_k} \;+\; \gamma_{ijkl} \frac{\partial^2 b_{0j}}{\partial x_k \partial x_l} \;+\; \ldots \tag{1.12}$$

1.2.4 Time-scale for flux expulsion

Expulsion of magnetic flux occurs at high R_m in closed streamline flows (Weiss, 1966; Parker, 1979). If the flow consists of neighboring cells, the field is then confined to intense flux sheets or ropes within a boundary layer at the cell walls. Field strengths within the sheet are by flux conservation of the order $O(R_m^{1/2} b_0)$ for a two-dimensional flow where b_0 is the magnitude of the initially imposed field. As the fluid motions advect magnetic flux tubes, tubes of opposite polarity are brought together resulting in reconnection. The length scale of the field also decreases so that ohmic dissipation of the field occurs even for small diffusivities. This hydromagnetic effect is reminiscent of the damping of electromagnetic radiation in a conducting solid wherein an impinging alternating magnetic field is damped by induced currents and confined to a skin depth of $\sqrt{\frac{2\eta}{\omega}} \sim R_m^{1/2} L$, η being the magnetic diffusivity and ω the radiation frequency (Jackson, 1975). Weiss (1966) determined the time required for flux to be expelled from the central region of a planar flow with closed streamlines and found it to be $O(R_m^{1/3} t_U)$, t_U being the convective timescale of the motion.

1.2.5 Self-consistent dynamos

Inclusion of the Lorentz force into the Navier-Stokes equation and the simultaneous solving of it with the induction equation constitutes the dynamical problem. An early attempt at a solution was made by Bullard and Gellman (1954) using poloidal and toroidal expansions of both the magnetic and velocity fields. However the the terms did not converge. Other dynamical models have used simpler solid dics. In these dynamos, the torque equation and Kirchhoff formulae are jointly solved. Similar models can produce reversals of the magnetic field by including a shunt device (Robbins, 1977) or by having two coupled discs (Rikitake, 1958; Cook and Roberts, 1970). It is interesting to note that Knobloch showed that the shunted disc model when cast into dimensionless form yields the Lorenz equations.

Hydromagnetic dynamical models are far more complicated than disc dynamos as one is dealing with a greater number of degrees of freedom. To date, no one has solved the complete set of equations simultaneously. However, the steady-state case has been studied numerically for the solar dynamo (Gilman and Miller, 1981; Gilman, 1983; Glatzmaier, 1984). as well as the geodynamo (Bullard and Gellman, 1954; Kropachev, 1971; Fearn and Proctor 1984, 1986b). In these examples, self-consistent velocity and magnetic fields are derived iteratively from some initial guesstimates of their forms. Such models do provide insights into field structure yet do not include magnetic field reversals. A question arises as to whether the equilibrium configurations so derived are physically attainable starting from an initially small magnetic field. A phenomenological model employing an alpha effect (to be discussed below) dependent on magnetic field intensity with a cutoff was recently developed by Olson and Hagee (Olson and Hagee, 1991).

Other dynamical models using truncated forms of the complete dynamo equations have been analysed in the context of solar magnetism (Catteneo, 1988) as well as smoothed models of spatially periodic flows for planetary dynamos (McMillan, 1988). Stability and bifurcation analysis of such systems provide information detailing the parameter range over which one should expect dynamo action. Such low-order models yield insights into the physically realistic dynamos of the future.

1.2.6 Types of dynamo models

A hydromagnetic dynamo necessarily involves a positive feedback mechanism. Two basic types of dynamos arise from this requirement. In a spherical geometry, toroidal fields serve as a source for poloidal field via the alpha effect. In turn, meridional field lines are deformeed to regenerate azimuthal fields against Ohmic decay. In the presence of large-scale azimuthal motion, the ω effect generates toroidal field lines, while small-scale helical motions producing an α effect recreate the poloidal field. This

is an $\alpha\omega$ dynamo. These models generally produce oscillatory (ac) dipolar fields. If in addition to the toroidal flow there is also large-scale meridional circulation , the m effect is included, thereby producing an $\alpha\omega$m dynamo. Models exploiting both α and ω effects to generate toroidal fields are $\alpha^2\omega$ type dynamos (Hagee and Olson, 1991). The present model is an α^2 dynamo.

1.3 Outline of the text

The present work investigates dynamo action in a spatially periodic flow studied by G.O. Roberts within a dynamical setting. This represents an extension of dynamo modelling beyond the purely kinematic approach. The objective is to provide a tractable model sufficiently flexibile as to apply to a range of possible conditions within planetary cores. Emphasis will be placed however on the geodynamo.

The outline of this dissertation is as follows. In Chapter two, details of the fluid motion are presented. I develop the form of the Roberts cell flow needed for the model. Fluid dynamical quantities such as the vorticity, circulation, helicity, and turnover time along streamlines are calculated. Symmetries of the flow are studied from the viewpoint of group-theoretical methods. Insights into the behavior of the flow under translation and rotation are made using these techniques.

Chapter three presents a simple kinematic dynamo model in which the fluid motion is the Roberts cell flow. The local magnetic Reynolds number R_m is low so that the dynamical effects may be neglected but the large-scale $R_m >> 1$ allowing for a net growth of the mean magnetic field. This is a simpler problem that the dynamical case and should be shown first. Also, the kinematic problem will allow the develpoment of results that carry over into the dynamical model.

In chapter four the main result, a dynamical model, is developed. The mean-field induction equation is obtained by calculating the alpha effect by a boundary layer analysis similar to Childress' (1979). This method applies at large magnetic

Reynolds number. Additionally, globally averaged axial torque and force balances from the Navier-Stokes equation, including the Lorentz force , are derived. In this model, the shape of the pathlines remains unaltered with only the velocity amplitudes affected as a result of the magnetic feedback. A set of three nonlinear scalar first-order ordinary differntial equations are derived detailing the temporal evolution of the mean magnetic field energy density and the axial and planar velocity amplitudes.

The requirement that the flow field form be maintained is unphysical but necessary for tractability. Under magnetic stresses, streamlines would deviate from the Roberts cell flow form. Nonetheless, the model does represent an improvement over purely kinematic dynamos and preserves essential physical content.

In chapter five the equations are recast into nondimensional form using system scale-lengths such as the cell size, the diffusive and and turnover times. Four parameters related to the magnetic Reynolds number, alpha effect coefficient and viscosities arise from the nondimensionalization process. I then seek steady-state solutions of the system and employ stability theory to ascertain the growth rates of the fields for small perturbations from equilibrium. Also the system's bifurcations can be found from the equilibria. Growth rates will depend on the given range of parameters and coincide with the bifurcation structure. Of particular interest are the Hopf bifurcations that occur along the upper subcritical branch. Robbins (1977) suggests the geodynamo operates subcritically.

Numerical integrations of the equations are performed using a multidimensional Runge-Kutta routine. Evolving the equations allows for a view of magnetic field growth for large initial deviations from equilibrium as well as for studying the growth in the region about the Hopf bifurcation. It is found that the oscillations grow until a limit cycle is encountered.

Finally, the issue of the geodynamo will be discussed in chapter six. The relevance of the assumption of spatially periodic motion to describe the liquid core's convection

will be elaborated, and parameters critical to the geomagnetic field expounded. Such a topic is of course rather speculative as the fluid motions within the core have yet to be completely discerned. Thus with those limititations I conclude the dissertation with a critique of the model.

All programs used to generate plots were written in Fortran 77 and run on the University of Hawaii VAX II system. Figures in the text were made using the DISSPLA library of Fortran graphics subroutines.

Chapter 2

CHARACTERISTICS OF ROBERTS CELL MOTION

2.1 Introduction

Spatially periodic motions in a conductive fluid can produce α^2 dynamos. One such flow, the Roberts cell, has been the focus of several aforementioned studies in a kinematic context. This chapter covers the fluid mechanical preliminaries by detailing relevant aspects of the motion, thereby laying a foundation for subsequent chapters in which the dynamo problem *per se* is addressed.

2.2 Prelimanary formalism

Functions periodic in space and/or time arise frequently in hydrodynamics, e.g., streamfunctions describing motion in Rayleigh convection, vortex streets, and Bénard cells. It is appropriate therefore to provide a formal setting and elucidate some useful results regarding such functions.

Let $\mathbf{R^m}$ denote the m-dimensional real space endowed with the standard Pythagorean metric and $\mathbf{Z}$ the set of integers. Further, let $\{\vec{l}_i\}_{i=1}^{m}$ be a set of linearly independent vectors spanning $\mathbf{R^m}$ i.e., a basis set (Apostol, 1969). An n-dimensional periodic function $\vec{f}(\vec{x} \in \mathbf{R^m})$ is a mapping $\vec{f} \; : \; \mathbf{R^m} \rightarrow \mathbf{U} \subset \mathbf{C^n}$ with the translational

property (cf. Roberts, 1970)

$$\vec{f}(\vec{x}) \;=\; \vec{f}(\vec{x} \;+\; \sum_{i=1}^{m} c_i \vec{l}_i),\; c_i \in \mathbf{Z}\; \forall\; c_i. \tag{2.1}$$

One can also define an inner product and consequently a norm and metric on the space S of such functions. The space S is then a Hilbert space as each element can be a limit of a Cauchy sequence i.e., $\lim_{n\to\infty} \parallel f_n - f \parallel = 0,\; f_n \in S$ where $\parallel \cdot \parallel$ is the norm.

The average of $\vec{f}(\vec{x})$ is determined over a single 'cell' **D** consisting of the region bounded by the parallelpiped formed by $\{\vec{l}_i\}$. Denoting the average by $< \vec{f} >$,

$$< \vec{f} > \;=\; \frac{1}{V} \int \cdots \int_{cell} \vec{f}(\vec{x}) \prod_{i=1}^{m} dx_i \text{ where V is the cell volume.} \tag{2.2}$$

Equation 2.1 is readily seen to be equivalent to $< \vec{f} > \;=\; \int_0^1 \cdots \int_0^1 \vec{f}(\sum_i \sigma_i \vec{l}_i) \prod_i d\sigma_i$ (Roberts, 1970) by noting that the determinant of the Jacobian matrix is the volume.

For $\vec{f}$ periodic, the wavevectors are drawn from the set $K \;=\; \{2\pi (J^T)^{-1}(c_1, \cdots, c_m) \mid c_i \in \mathbf{Z}\}$ where $J_{ij} \;=\; (l_j)_{x_i}$ is the Jacobian matrix mentioned above. One has the following results

$$\vec{f}(\vec{x}) \;=\; \sum_{\vec{k}\in K} \vec{a}(\vec{k}) \exp^{i\vec{k}\cdot\vec{x}} \text{ with } \vec{a}^*(\vec{k}) \;=\; \vec{a}(-\vec{k}), \tag{2.3}$$

$$< \vec{f} > \;=\; \vec{a}(0), \tag{2.4}$$

$$\text{For } \sum_i n_i \neq 0,\; < \partial_{x_1}^{n_1} \cdots \partial_{x_m}^{n_m} \vec{f} > \;=\; 0, \tag{2.5}$$

$$< \nabla \vec{f} > = < \nabla^2 \vec{f} > \;=\; 0. \tag{2.6}$$

Equations 2.3-2.4 are standard, while (2.5) is obtained by noting that the $\vec{k} \;=\; 0$ term will be zero; equation 2.6 is a corollary of (2.5).

2.3 Development of the model flow

2.3.1 Stream function and velocity field

In order to describe a plausible viscous flow, the stream function should be continuous through the second partial derivatives, i.e., $\psi \in \mathbf{C^2(D)}$ where $\mathbf{D}$ is the region containing the fluid. This is evident by the requirement that the flow be smooth as viscosity weakens velocity gradients. The model developed below satisfies this requirement, as well as the looser conditions for an inviscid flow.

I begin with the stream function given in dimensional form by

$$\psi = \frac{U}{k} \sin kx \sin ky. \tag{2.7}$$

For planar motion equation 2.7 describes a Kolmogorov flow. Its simplicity makes the flow amenable to smoothing and perturbation analysis and thus is particularly appealing. Rolls in Rayleigh convection have similar patterns so the flow is a useful modelling tool.

In the form used here, $\mid \psi \mid \leq \frac{U}{k}$. Horizontal velocities derive from the stream function and are tangent to streamlines (Tritton, 1987). The velocity field satisfies the incompressibility condition. A graph of the Kolmogorov flow streamlines is presented in Figure 2.1.

$$\vec{u}_H = u(x,y)\,\hat{x} + v(x,y)\,\hat{y}, \tag{2.8}$$

$$u(x,y) = \frac{\partial \psi}{\partial y}, \quad v(x,y) = -\frac{\partial \psi}{\partial x} \tag{2.9}$$

$$\nabla \cdot \vec{u}_H = 0. \tag{2.10}$$

Adding a z-velocity $u_z = w(\psi)$ retains much of the structure found in two dimensions, as particle motion is still constrained to the concentric cylindrical stream surfaces $\psi = constant$ and the velocity field remains solenoidal. Such flows are quasi two-dimensional and constitute exact solutions of the Euler equation (Bayley, 1987). This is Roberts' cellular flow.

Solenoidal vector fields may be decomposed into toroidal and poloidal components (Parker, 1979). A similar construct is obtained here whereby

$$\vec{u} = \nabla \times \psi\hat{z} + \nabla \times \nabla \times W\hat{z}, \quad \nabla^2 W = w. \tag{2.11}$$

From the velocity structure, the particle motion is evident; fluid particles move along nested helices within square cells as shown in Figure 2.2. Streamlines in Figure 2.1 are the projections of pathlines onto the x-y plane. Note that the axial velocity remains constant along streamsurfaces, yet allows for vertical shear. This last feature is reminiscent of the Taylor-Proudman theorem for inviscid rotating systems.

Stagnation points, where $\vec{u} = 0$, form a square lattice on the x-y plane at the positions indicated below. Separatrices, given by $\psi = 0$, connect the stagnation points and form cell boundaries.

$$\vec{u} = 0 \text{ at } \{\frac{\pi}{k}(n_1, n_2) \mid n_1, n_2 \in \mathbf{Z}\} \tag{2.12}$$

2.3.2 Vorticity and helical structure

Vorticity, defined as the curl of the Eulerian velocity field, represents a measure of the rotationality of a flow. A sufficient condition for nonzero vorticity is that a fluid element changes its orientation while executing its translational motion in the fluid (Tritton, 1987).

By Stokes' Law the surface integral of the vorticity equals the line integral of the velocity along a closed curve. This is Kelvin's Circulation Theorem (Chandrasekhar, 1961). The circulation is defined below.

$$\Gamma = \int\int_S \nabla \times \vec{u} \cdot d\vec{S} = \oint_{\partial S} \vec{u} \cdot d\vec{l} \tag{2.13}$$

All flows with closed streamlines possess nonzero circulation. The converse statement, however, is not generally true as seen in the case of simple shear flows (Tritton, 1987).

In the case of quasi two dimensional flows i.e., $\vec{u} = \nabla \times \psi\hat{z} + f(\psi)\hat{z}$ vorticity and circulation are given, respectively, by

$$\vec{\omega} = \nabla^2\psi\hat{z} - \frac{df}{d\psi}\vec{u}_H, \tag{2.14}$$

$$\Gamma = \int\int_S \nabla^2\psi dS. \tag{2.15}$$

For the Roberts cell flow defined above

$$\Gamma = 2k^2 \int\int_{cell} \psi dS = \frac{8U}{k}. \tag{2.16}$$

Helicity indicates the 'handedness' of a vortex as well as the knottedness of vortex filaments (Zeldovich et al., 1983). It is defined as the surface integral of the scalar product of vorticity and velocity.

$$H = \int\int \vec{u} \cdot \vec{\omega} dS \tag{2.17}$$

As defined, H is a pseudoscalar quantity, changing signs upon coordinate inversion. Helical flows lack reflectional symmetry and are prime candidates for dynamo action (Moffatt, 1978), yet nonhelical flows may also regenerate magnetic fields (Gilbert, Frisch, and Pouquet, 1988). Purely planar flows are incapable of supporting dynamo action due to the absence of a feedback mechanism. This necessity of a third velocity component coupled with the nonreflectional symmetry of the flow causes the Roberts cell motion to be helical. To be specific, the helicity is nonzero when integrated over many cells if the axial velocity is an odd function of the stream function (for quasi-two-dimensional flows),

$$u_z = w(\psi) \text{ with } w(-\psi) = -w(\psi). \tag{2.18}$$

This last statement is equivalent to saying the flow possesses a definite helicity (our present model is right-handed).

Flows of maximal helicity are Beltrami fields (Childress, 1988), where the velocity and vorticity are parallel ($\vec{\omega} = c(\vec{x})\ \vec{u}$). Perkins and Zweibel (1987) considered a

restrictive scaling on the axial velocity amplitude to retrieve the Beltrami property for a purely kinematic Roberts cell dynamo. The Roberts cell version in the present study with $w(\psi) = K\ \psi$ exhibits af 'quasi-Beltrami' property in that the velocity can be divided into two components with the curl of one being parallel to the other i.e.,

$$H = KU^2 \int_0^{\frac{\pi}{k}} \int_0^{\frac{\pi}{k}} [\sin^2 kx \sin^2 ky] dxdy = \frac{\pi^2 KU^2}{k^2}, \tag{2.19}$$

$$\nabla \times \vec{u}_H = \frac{2k^2}{K} \vec{u}_V, \tag{2.20}$$

$$\nabla \times \vec{u}_V = K\vec{u}_H. \tag{2.21}$$

2.3.3 Turnover time and Lagrangian motion

Particles are affixed to stream surfaces for steady flows so turnover time depend solely on values of ψ. We employ the symmetry of the motion to derive expressions for the period and particle positions as a function of time. Assume a fluid particle is initially at $y = \frac{\pi}{2k}, x = \frac{1}{k} \arcsin \tilde{\psi}_0$ in the cell S defined in Figure 2.1. The time required to reach $x = \frac{\pi}{2k}$ is $\frac{T}{4}$ where T is the turnover time along the particular streamline. To obtain an expression for the turnover time one determines the equation of motion for a given particle which is the Lagrangian description of motion. This procedure yields the turnover time in terms of an incomplete elliptic integral of the first kind, similar to that derived for the harmonic oscillator problem

$$\vec{x} = \vec{x}(\vec{a}, t) \text{ where } \vec{x}(\vec{a}, 0) = \vec{a}, \tag{2.22}$$

$$\frac{d^2x}{dt^2} = \frac{1}{2} kU^2 \sin 2kx \implies \frac{\dot{x}^2}{2} - \frac{1}{2} U^2 \sin^2 kx = E, \tag{2.23}$$

$$\frac{d^2y}{dt^2} = \frac{1}{2} kU^2 \sin 2ky, \tag{2.24}$$

$$z = w(\psi)t. \tag{2.25}$$

The x-velocity is zero at time t = 0, so we obtain $E = -\frac{1}{2}U^2\tilde{\psi}_0{}^2$ where $\tilde{\psi}_0 = \sin kx \sin ky$. Now the equation for the turnover time is given by

$$T = \frac{4}{kU|\tilde{\psi}_0|}\int_{\theta_0}^{\frac{\pi}{2}} \frac{d\theta}{\sqrt{\frac{1}{\tilde{\psi}_0^2}\sin^2\theta - 1}} \quad \text{where } \theta_0 = \arcsin\tilde{\psi}_0. \tag{2.26}$$

Figure 2.3 displays the period as a function of $\tilde{\psi}_0$.

Two cases of interest immediately arise from the above equation. First, near the vortex centers (i.e., $|\tilde{\psi}_0| = 1 - \epsilon^2$), trajectories approximate circles in the x-y plane. This reduces the period expression to one involving the parameter r, the radius of the streamline as measured from the cell center.

$$\tilde{\psi}_0 = \sin[\frac{\pi}{2} + k\delta_x]\sin[\frac{\pi}{2} + k\delta_y] \approx 1 - \frac{k^2}{2}(\delta_x{}^2 + \delta_y{}^2) = \frac{k^2}{2}r^2, \tag{2.27}$$

$$|\vec{u}| \approx Ukr,\ T \approx \frac{2\pi}{kU}. \tag{2.28}$$

Also of interest is the situation of small $\tilde{\psi}_0$ near the cell boundary. Here the turnover time increases without bounds due to the stagnation points. As will be seen, the magnetic field will be confined primarily to this region.

Employing the expression derived above the $x-$position as a function of time is given by

$$\int_{\arcsin\tilde{\psi}_0}^{kx(t)} \frac{d\theta}{\sqrt{\frac{1}{\tilde{\psi}_0^2}\sin^2\theta - 1}} = Uk\tilde{\psi}_0 t. \tag{2.29}$$

The $y-$ position of the fluid particle is then found from the stream function:

$$y_L = \frac{1}{k}\arcsin(\frac{\tilde{\psi}_0}{\sin kx}) \text{ along the lower half of a stream line,} \tag{2.30}$$

$$y_U = \frac{\pi}{k} - y_L \text{ along the upper half of a streamline.} \tag{2.31}$$

A plot of $x(t)$ versus t is shown for a typical streamline $\tilde{\psi}_0 = 0.5$ in Figure 2.4. Note that the presence of stagnation points increases transit times around the 'corner' regions $x = \frac{\pi}{4k}, \frac{3\pi}{4k}$.

2.4 Flows and symmetries

Recent studies (cf. Zaslavskii et al., 1991) have shown an underlying structural similarity in many patterns of physical interest. Consider the set of unit vectors $E_q = \{\hat{e}_j\}_{j=1}^{q}$ forming a q-star in the x-y plane, i.e.,

$$\hat{e}_j = (\cos\frac{2\pi j}{q}, \sin\frac{2\pi j}{q}). \tag{2.32}$$

The stream functions ψ_q defined by

$$\psi_q = \psi_0 \sum_{j=1}^{q} \cos(\hat{e}_j \cdot \vec{r}), \tag{2.33}$$

where $\vec{r} = (x, y)$ form an exact solution of the steady, Euler equation. For $q = 2$ the streamfunction describes the Kolmogorov flow, a simple shearing motion. The $q = 3, 6$ cases yield hexagonal cells. For the case of $q = 4$ a square cell pattern emerges and It is readily verifible that the form is identical to the streamfunction listed above with rotation, translation, and change of scale. Symmetries of orders $q = 3, 4, 6$ mimic the regular polygons capable of tiling a plane. For $q \neq 2, 3, 4, 6$ the streamlines have a quasicystal pattern (Q-flows) in which long-range order is lost. A related result from group theory is that translational symmetry is consistent only with rotations of $2\pi/n$ where n= 1,2,3,4,6.

2.4.1 Group properties of the flow

The symmetry group of a square, D_4 in the Schoenflies notation or 422 in the crystallographic notation (Falicov, 1966), contains 8 elements and is isomorphic to a subgroup of P_4, the permutations of 4 elements. Group elements are expressed as combinations of the two generators r, s and are listed in Table 2.1.

The first column is the group element. The second column gives the counterclockwise rotation (in degrees) and axis. The last two columns are the P_4 element isomorph and cyclic structure, respectively.

Table 2.1: Group elements in D_4

g_i	rotation	P_4	cycle structure
i	-	[1234]	(1)(2)(3)(4)
r	90°_z	[4123]	(1234)
r^2	180°_z	[3412]	(13)(24)
r^3	270°_z	[2341]	(1234)
s	180°_x	[4321]	(14)(23)
sr	$180^\circ_{x=-y}$	[3214]	(13)(2)(4)
sr^2	180°_y	[2143]	(12)(34)
sr^3	$180^\circ_{x=y}$	[1432]	(1)(3)(24)

Group elements may be combined into classes, each class containing elements with similar cyclic structure (Matthews and Walker, 1970). For the group D_4 the classes are reproduced with a notation change from (Falicov, 1966) in Table 2.2.

It is now possible to construct a character table of the group. Characters are the traces of the matrices forming the irreducible representations of the group. An important result from group theory is that the number of irreducible representations equals the number of classes (Falicov, 1966). Irreducible representations of the group members are shown in Table 2.3 and the character table for D_4 is given in Table 2.4 with notational changes from (Falicov, 1966). Characters are denoted by the μ_i.

Under a group element R, a function transforms according to the rule (Falicov, 1966)

$$\hat{P}_R\, f(\vec{x}) \;=\; f(R^{-1}\vec{x}),\;\; R^{-1}(x,y,z) \;=\; (Rx, Ry, Rz). \tag{2.34}$$

I derive in table 2.5 transformations of the Roberts cell stream function under the action of group rotations. The identity element i is omitted as it leaves a function unchanged.

Table 2.2: Classes of the group D_4

class	group elements
C_1	i
C_2	r , r^3
C_3	r^2
C_4	s , sr^2
C_5	sr , sr^3

From Table 2.5, $\sin x \sin y$ transforms according to representation 4 (as determined by looking at the elements r and s in Table 2.3) , i.e., it is antisymmetric with respect to both a rotation of$\pi/2$ about the z-axis and a rotation of π about the x- and y-axes. Whence when acted upon by either of the group elements r and s the function transforms into $-\sin x \sin y$. The function is an eigenfunction of the operators r and s. However, centering the origin in the middle of the square cell without rotation symmetrizes the streamfunction, i.e, $\psi = \cos x \cos y$ transforms under representation 1. Translating the origin by a quarter wavelength on either the x or y axis yields $\psi = \cos x \sin y$, $\sin x \cos y$ respectively, which transform by representation 5.

I also investigated related functions. The functions $\sin^2 x \cos^2 y \pm \cos^2 x \sin^2 y$, $\cos x \pm \cos y$ transform according to representations 1 (for the '+') and 3 (for the '-'). The functions $\sin x \pm \sin y$ transform according to representation 5, while $\sin x \pm \cos y$, $\cos x \pm \sin y$ exhibit a mixed symmetry containing both representations 1 and 3.

For representation 2, the picture is complex. In this representation, the transformation is symmetric under rotations about the z-axis, but antisymmetric with respect to all other operations (which involve rotations of π about axes in the x-y plane). The only function in this representation in Table 5 is $\psi = z$. So any function transforming by representation 2 wil be of the form $f(x, y, z) = g(z)h(x^2 + y^2)$ where $g(\cdot)$ is

Table 2.3: Irreducible representations of the group elements

element	representation				
	1	2	3	4	5
i	1	1	1	1	$\begin{pmatrix} 1 & 0 \\ 0 & 1 \end{pmatrix}$
r	1	1	-1	-1	$\begin{pmatrix} 0 & -1 \\ 1 & 0 \end{pmatrix}$
r^2	1	1	1	1	$\begin{pmatrix} -1 & 0 \\ 0 & -1 \end{pmatrix}$
r^3	1	1	-1	-1	$\begin{pmatrix} 0 & 1 \\ -1 & 0 \end{pmatrix}$
s	1	-1	1	-1	$\begin{pmatrix} 1 & 0 \\ 0 & -1 \end{pmatrix}$
sr	1	-1	-1	1	$\begin{pmatrix} 0 & -1 \\ -1 & 0 \end{pmatrix}$
sr^2	1	-1	1	-1	$\begin{pmatrix} -1 & 0 \\ 0 & 1 \end{pmatrix}$
sr^3	1	-1	-1	1	$\begin{pmatrix} 0 & 1 \\ 1 & 0 \end{pmatrix}$

Table 2.4: Character table for D_4

character	class				
	C_1	C_2	C_3	C_4	C_5
μ_1	1	1	1	1	1
μ_2	1	1	1	-1	-1
μ_3	1	-1	1	1	-1
μ_4	1	-1	1	-1	1
μ_5	2	0	-2	0	0

Table 2.5: Transformation table

function	group element						
	r	r^2	r^3	s	sr	sr^2	sr^3
x	-y	-x	y	x	-y	-x	y
y	x	-y	-x	-y	-x	y	x
z	z	z	z	-z	-z	-z	-z
sinxsiny	-sinxsiny	sinxsiny	-sinxsiny	-sinxsiny	sinxsiny	-sinxsiny	sinxsiny
cosxcosy	cosxcosy	cosxcosy	cosxcosy	cosxcosy	cosxcosy	cosxcosy	cosxcosy
sinxcosy	-sinycosx	-sinxcosy	sinycosx	sinxcosy	-sinycosx	-sinxcosy	sinycosx
cosxsiny	cosysinx	-cosxsiny	-cosysinx	-cosxsiny	-cosysinx	cosxsiny	cosysinx

an odd function. As I was looking for periodic functions of x, y only, I conclude that no such function invariant under representation 2 exists.

2.5 Chapter summary

In this chapter, the stream function for the Roberts square cell flow was presented and the fluid dynamical quantities of interest such as vorticity, circulation and helicity were calculated. It is seen that the flow is helical with a 'quasi-Beltrami' nature depending on the choice of the axial (z-direction) velocity. To insure a nonzero helicity, I showed that a sufficient condition in the axial velocity being an odd function of ψ.

Using group-theoretical methods I determined equivalent forms of the streamfunction. These forms are also obtainable by coordinate translations, which follows from a basic theorem in group theory. I found that the resulting functions transformed according to representations 1, 3, 4, and 5 of the group D_4. No function $f(x, y)$ seems invariant under representation 2. As this representation involves inversion of the z-axis with rotations in the x-y plane, any function transforming by representation 2 must be antisymmetric in z and symmetric in x and y.

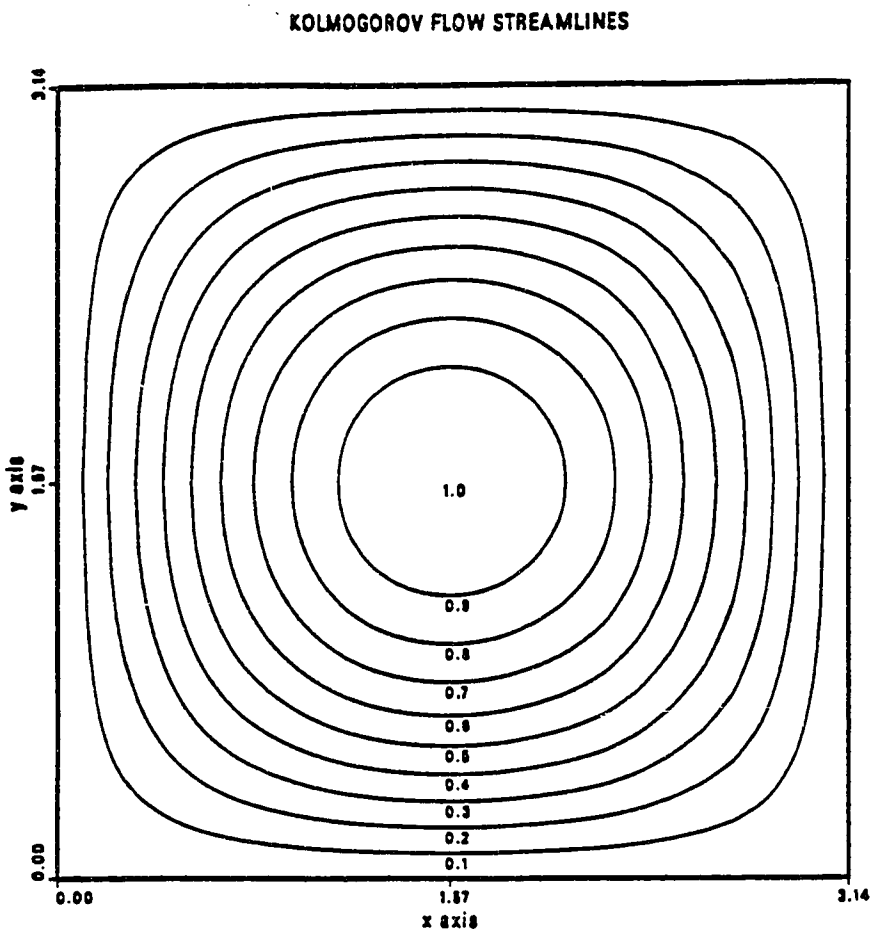

Figure 2.1: The Kolmogorov flow streamlines

Streamlines $\tilde{\psi}_0 = \sin kx \sin ky$ are given for $0 \leq \tilde{\psi}_0 \leq 1$ in increments of 0.1, corresponding to the square cell $S = \{(x, y) \mid 0 \leq x, y \leq \frac{\pi}{k}\}$.

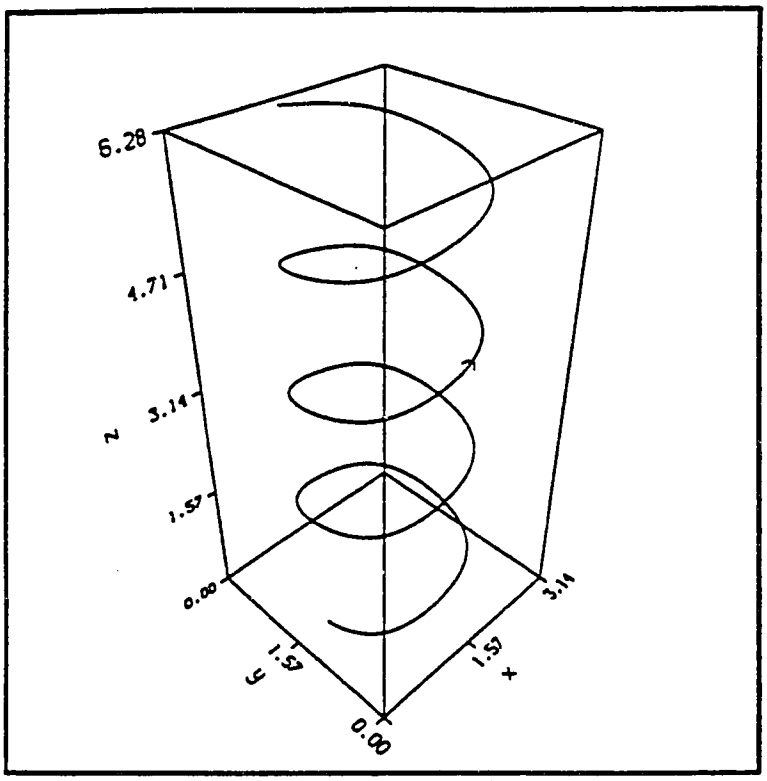

Figure 2.2: Typical pathlines in the Roberts cell flow

Pathlines consist of nested helices bounded by the surface $\psi(x,y) = 0$. Particle trajectories are indicated by arrows. For the pathline given, $w = 0.4\tilde{\psi}_0$

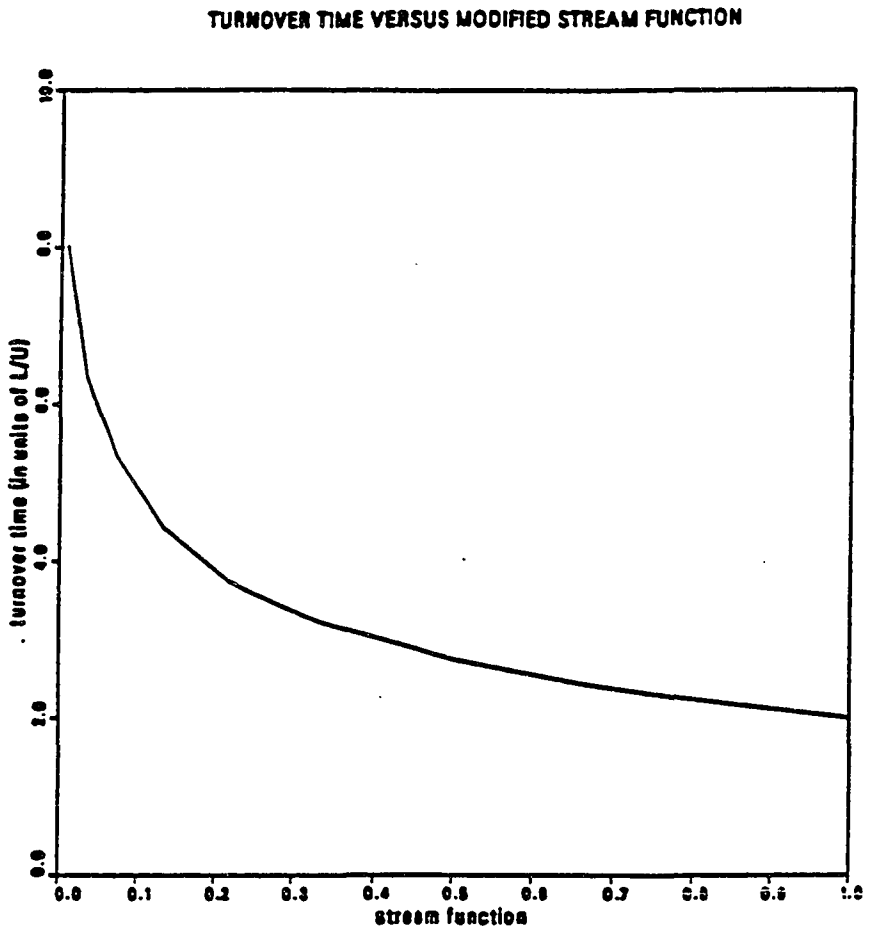

Figure 2.3: Dependency of the turnover time on the stream function

Turnover time $T(\tilde{\psi}_0)$ is calculated from equation 28. As $\tilde{\psi}_0 \to 0$, $T \to \infty$ due to the corner stagnation points.

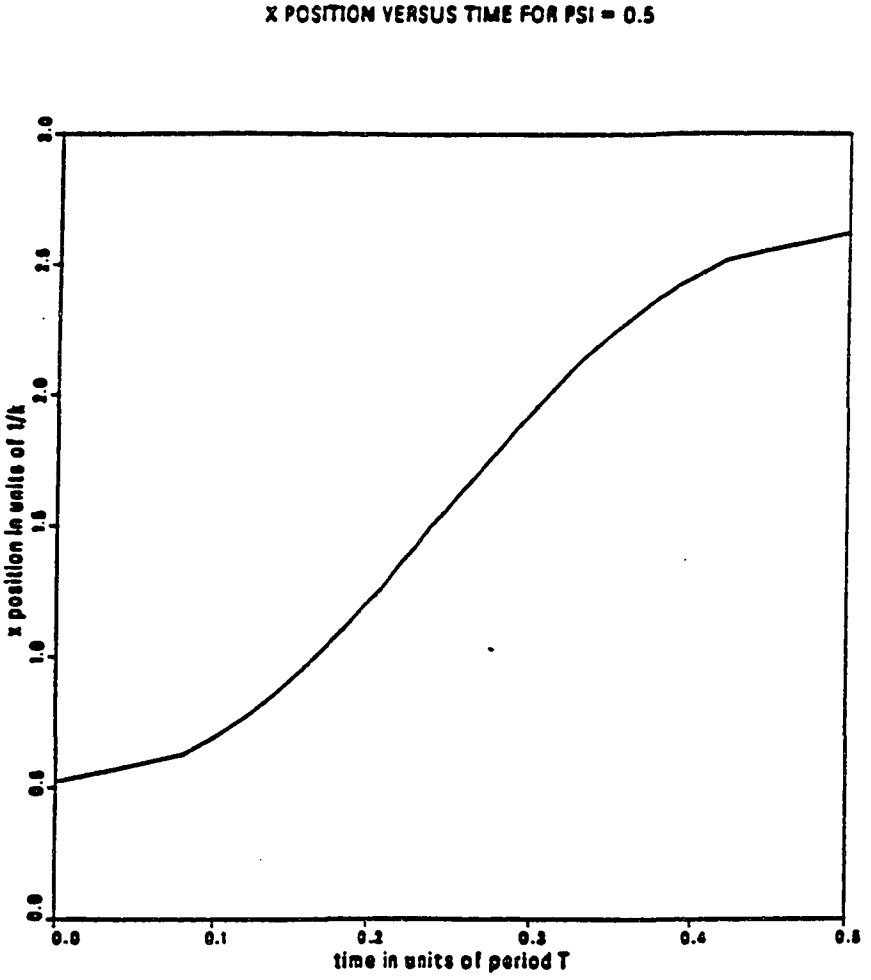

Figure 2.4: Position versus time along a typical streamline

The x-position is plotted versus time in units of the turnover time for $\tilde{\psi}_0 = 0.5$ for one-half cycle The initial position $x_0 = k^{-1} \arcsin(\tilde{\psi}_0)$. The final position $= \frac{\pi}{k} - x_0$.

Chapter 3

LOW R_m INDUCTION IN THE MODEL FLOW

3.1 Chapter overview

Faraday's law coupled with Ohm's and Ampere's laws yield the hydromagnetic induction equation. The kinematic dynamo problem, valid for weak magnetic field strengths, utilizes only the induction equation and is the theme of this chapter. Several results, namely induction at low magnetic Reynolds numbers and the minimum criterion for mean-field dynamo action, are developed herein.

3.2 First order smoothing at low R_m

3.2.1 Preliminary considerations

I begin the investigation of dynamo action in the Roberts cell flow by considering induction in the case of small magnetic Reynolds numbers. Recall that R_m is a measure of the relative strengths of advection and diffusion of a magnetic field within a fluid. For a fluid of uniform conductivity σ, a typical lengthscale l and velocity amplitude U the magnetic Reynolds number is $R_m = \frac{Ul}{\eta}$ where $\eta = (\mu\sigma)^{-1}$.

A small value (< 1) of R_m implies that diffusive effects dominate. Under such conditions, local (small-scale) magnetic field lines decay unless maintained by some external source. One could imagine, for example, a fluid at low R_m being placed

between the poles of a magnet. Within the fluid, the magnetic field would eventually be stationary, in which case the advection of the imposed field just balances diffusion. The spatial distribution of the field would reflect the nature of the fluid motion.

Consider the Roberts cell motion in the case of small R_m. To expedite the calculation of the alpha effect, we employ the two-scale (mean-field electrodynamic) approach mentioned earlier. Further it shall be noted that the average of a quantity shall be taken over four cells constituting a complete "cycle" of the motion in the x-y plane, that is,

$$< f >= \frac{1}{4l^2} \int_0^{2l} \int_0^{2l} f(\vec{x}, t) dx dy \tag{3.1}$$

where l is the cell dimension. The modified stream function is now

$$\psi = \frac{Ul}{\pi} \sin \frac{\pi x}{l} \sin \frac{\pi y}{l}. \tag{3.2}$$

Equivalently, the wavenumber now equals $k = \frac{\pi}{l}$.

Small-scale magnetic fields will have the same periodicity as the flow due to the translational symmetry of the system. This is seen by considering a *gedanken* experiment. A uniform externally applied magnetic field $\vec{b}_0$ is embedded in a stationary fluid. At time t=0 the Roberts cell motion begins. The field twists, causing the formation of cell-sized perturbations. Put differently, the field is now considered as consisting of the mean portion $\vec{b}_0$ and a fluctuation $\vec{b}'$. Since alternating cells behave identically, the perturbation likewise possesses the flow's periodicity. One can employ order-of-magnitude arguments to facilitate in the computation of the fluctuating field. The temporal evolution of the perturbing field is given by

$$\frac{\partial \vec{b}'}{\partial t} = \nabla \times \vec{u}' \times (\vec{b}_0 + \vec{b}') + \eta \nabla^2 \vec{b}', \tag{3.3}$$

$$\nabla \cdot \vec{b}' = 0 \tag{3.4}$$

$$\vec{b}'(\vec{x}, 0) = 0. \tag{3.5}$$

It is evident that the term $\nabla \times (\vec{u}' \times \vec{b}')$ is the most difficult to handle. To solve for $\vec{b}'$ exactly would require expressing the field as an infinite Fourier sum over modes with the flow's periodicity. Then matching exponents in the induction equation would determine conditions on the Fourier amplitudes $\hat{b}(\vec{k})$. If some simplifying assumptions are possible, the perturbed electromotive force term may be omitted altogether.

First-order smoothing (Moffatt, 1978) provides such a simplification. Each term in the induction equation can be assigned an order-of-magnitude value; some terms are larger than others. If the offending term is smaller than either $\partial_t \vec{b}'$ or $\eta \nabla^2 \vec{b}'$ it could be dropped under first-order smoothing. The first choice doesn't involve the diffusivity (i.e., the magnetic Reynolds number) so we take the second choice. In the case of conventional turbulent motions $|\frac{\partial \vec{b}'}{\partial t}| \sim |\nabla \times \vec{G}| << |\eta \nabla^2 \vec{b}'|$. This analysis is valid for the low R_m regime. Besides, the α effect to be determined for mean field growth will use the steady-state value of the perturbed field.

$$\frac{u'b'}{l} < \frac{\eta b'}{l^2} \tag{3.6}$$

$$R_m = \frac{u'l}{\eta} << 1 \tag{3.7}$$

Here $l = \frac{\pi}{k}$ is the familiar cell wall length.

Two timescales, the convective time $t_u = \frac{l}{u}$ and the diffusive time $t_d = \frac{l^2}{\eta}$ are relevant. The magnetic Reynolds number may be considered as the ratio of these two times i.e., $R_m = \frac{t_d}{t_u}$.

After initial growth of the perturbing field, diffusion balances the restorative advection wrought by the mean field and $\vec{b}'$ achieves a steady-state ($t = \infty$) configuration. In this construct we maintain the 'weak field' assumption that the Lorentz force doesn't alter pathlines. Then the perturbed field satisfies

$$0 = \vec{b}_0 \cdot \nabla \vec{u}' + \eta \nabla^2 \vec{b}'. \tag{3.8}$$

For the right-hand terms to be of similar magnitude, the mean field amplitude

must exceed the perturbed field's amplitude by a factor of R_m^{-1},

$$O(\frac{\eta b'}{l^2}) \sim O(\frac{u' b_0}{l}), \tag{3.9}$$

$$b_0 \sim R_m^{-1} b' \text{ where } R_m << 1. \tag{3.10}$$

Now that the magnitude of the perturbed field relative to the mean field is established, it is useful to consider the mean field and ascertain its time- and length- scales. Evolution of the averaged magnetic field is governed by the induction equation

$$\frac{\partial \vec{b}_0}{\partial t} = \nabla \times < \vec{u} \times \vec{b}' > + \eta \nabla^2 \vec{b}_0, \tag{3.11}$$

where the α effect is the first term on the right-hand side. Allowing the length scale of the mean field to be denoted by L order-of-magnitude arguments show that for smallscale inductive effects to balance diffusion one must have

$$\frac{u R_m b_0}{L} \sim \frac{\eta b_0}{L^2}, \tag{3.12}$$

$$R_m R_L \sim O(1) \text{ where } R_L = \frac{uL}{\eta} \tag{3.13}$$

$$\frac{l}{L} \sim \sim R_L^{-2} \sim R_m^2 \tag{3.14}$$

From equations 3.12-3.14, it is seen that $L \sim R_m^{-2} l >> l$ which justifies the assumption of wide scale separation. Also, the largescale magnetic Reynolds number R_L is greater than one so that a mean field of lengthscale $O(R_m^{-2} l)$ may be destabilised by the α effect producing a dynamo.

Convective and diffusive timescales for the mean field may now be ascertained. In terms of the local diffusion time the largescale convective and diffusive times, respectively, are given by

$$t_u^L = \frac{L}{u} \sim R_m^{-3} t_d, \tag{3.15}$$

$$t_d^L = \frac{L^2}{\eta} \sim R_m^{-4} t_d. \tag{3.16}$$

Again the timescales relevant to the evolution of $\vec{b}_0$ are widely separated from those of $\vec{b}'$.

3.2.2 Calculation of the R_m order field

To solve for the perturbed field in the Roberts cell case, substitute the velocity $\vec{u} = U(\sin kx \cos ky, -\cos kx \sin ky, \frac{V}{U} \sin kx \sin ky)$ into the induction equation yielding

$$b'_x = \frac{U}{2k\eta}[b_{0x} \cos kx \cos ky - b_{0y} \sin kx \sin ky] \tag{3.17}$$

$$b'_y = \frac{U}{2k\eta}[b_{0x} \sin kx \sin ky - b_{0y} \cos kx \cos ky] \tag{3.18}$$

$$b'_z = \frac{V}{2k\eta}[b_{0x} \cos kx \sin ky + b_{oy} \sin kx \cos ky] \tag{3.19}$$

The perturbed magnetic field has the same periodic structure as the fluid. That the perturbed field satisfies Gauss' Law is readily verifiable. Further, the initial condition on $\vec{b}'$ is met by multiplying the above spatial components by $1 - \exp(-\eta k^2 t)$. The inclusion of the temporal factor overcomes objections that the above equations were time-independent and hence incorrect. Actually, The time derivative of $\vec{b}'$ could have been maintained in the modified induction equation, so long as the magnetic Reynolds number remained small. Once $\vec{b}'$ is known, the mean electromotive force is quickly calculated.

$$< \vec{u}' \times \vec{b}' > = \alpha \cdot \vec{b}_0, \tag{3.20}$$

$$\alpha_{ij} = -\frac{UV}{4k\eta}(1 - e^{-\eta k^2 t})\delta_{ij} \quad (i, j = 1, 2), \tag{3.21}$$

$$\alpha_{3j} = 0. \tag{3.22}$$

The 2×2 unit matrix δ_{ij} is the familiar Kronecker delta. No contribution to α is made by b_{0z} as the flow depends only on the planar coordinates x and y. The net small-scale emf, having formed, is capable of driving a current antiparallel to the mean field. Childress (1988) obtained a similar expression using a cellular flow with a different scaling than the present work, however he did not include the time dependence in his calculation of α. Nonetheless if one allows a sufficient time $t >> \frac{1}{\eta k^2}$ to pass, Childress' solution will be obtained.

3.2.3 Higher order field terms

It is of interest now to include the small-scale advective term in the induction equation and determine higher order terms in the perturbed magnetic field. To do this, I expand $\vec{b}'$ in a perturbation series, matching powers of the expansion coefficient R_m i.e.,

$$\vec{b}' = R_m\vec{b}_1 + R_m^2\vec{b}_2 + ... \tag{3.23}$$

Rewriting the induction equation in dimensionless form using the scaling $t = \frac{L^2}{\eta}t_d$, $\vec{u} = U\vec{u_d}$, $\nabla = \nabla_d$ where the subscript refers to dimensionless quantities yields

$$\frac{\partial\vec{b}}{\partial t_d} = R_m\nabla_d \times (\vec{u_d} \times \vec{b}) + \nabla_d^2\vec{b}. \tag{3.24}$$

Rewriting the induction equation in this manner yields an infinite set of iterative equations:

$$\frac{\partial\vec{b_1}}{\partial t} = \vec{b_0}\cdot\nabla\vec{u} + \nabla^2\vec{b_1}, \tag{3.25}$$

$$\frac{\partial\vec{b_2}}{\partial t} = \vec{b_1}\cdot\nabla\vec{u} - \vec{u}\cdot\nabla\vec{b_1} + \nabla^2\vec{b_2}, \tag{3.26}$$

$$\frac{\partial\vec{b_n}}{\partial t} = \vec{b}_{n-1}\cdot\nabla\vec{u} - \vec{u}\cdot\nabla\vec{b}_{n-1} + \eta\nabla^2\vec{b_n}. \tag{3.27}$$

In equations 3.25-3.27, the 'd' subscript was dropped for convenience. The solution of equation 3.25 was previously derived first-order smoothing results (3.17)-(3.19). In equation 3.26, we require the field $\vec{b_2}$ to be spatially periodic and solenoidal. Solving, it is found that

$$\vec{b_2} = \frac{U^2}{8k^2\eta^2}(b_{0x}\cos 2ky, b_{0y}\cos 2kx, \frac{V}{U}[b_{0x}\sin 2ky - b_{0y}\sin 2kx])(1 - 2e^{-2\eta k^2 t} + e^{-4\eta k^2 t}). \tag{3.28}$$

It is seen that the higher order corrections do not contribute to the mean small-scale electromotive force. i.e., $< \vec{u}' \times \vec{b}_n >= 0$ for $n > 1$. Also for each iterate $b_n \sim O(R_m^n b_0)$, Thus for small R_m, the first-order smoothing technique provides a sufficiently accurate picture of the perturbed magnetic field.

3.3 A mean field dynamo model

The determination of α in equations 3.20-3.22 can be employed to calculate the mean field growth rate, thereby creating a dynamo if the real part of that rate is positive. Implicit in the foregoing discussion was the assumption of the constancy of $\vec{b_0}$ over time- and length-scales describing the development of $\vec{b'}$ which was shown to be valid. Using the definition of an average $\vec{b_0}$, if allowed to vary, can depend only on z and t. It must however also satisfy Gauss' law, namely $\nabla \cdot \vec{b_0} = 0$. This constraint implies b_{0z} at most depends on time. Yet from the induction equation, the z-component satisfies $\partial_t b_{0z} = 0$, implying it is at most constant. We can therefore set it equal to zero without altering the physical content. Inserting the α effect into the mean-field induction equation leads to a pair of coupled differential equations for b_{0x} and b_{0y}.

$$\frac{\partial b_{0x}}{\partial t} = -\alpha \frac{\partial b_{0y}}{\partial z} + \eta \frac{\partial^2 b_{0x}}{\partial z^2} \tag{3.29}$$

$$\frac{\partial b_{0y}}{\partial t} = \alpha \frac{\partial b_{0x}}{\partial z} + \eta \frac{\partial^2 b_{0y}}{\partial z^2} \tag{3.30}$$

Both terms have the same time dependence and from separation of variables the temporal part is readily seen to be of the form $b_{0x}, b_{0y} \sim e^{pt}$. The growth rate p now can be determined. The spatial portion of the mean field admits a solution of the form $\sim e^{i\lambda z}$ where $\lambda \sim L^{-1}$. Using matrix notation, we determine the eigenparameter p,

$$0 = \begin{vmatrix} -\eta\lambda^2 - p & -i\alpha\lambda \\ i\alpha\lambda & -\eta\lambda^2 - p \end{vmatrix} \tag{3.31}$$

The mean field growth rate $p = \pm\alpha\lambda - \eta\lambda^2$ assumes its maximum value when $\frac{dp}{d\lambda} = 0$, yielding $p_{max} = \frac{\alpha^2}{4\eta}$. Varying on a scale λ^{-1} the magnetic Reynolds number based on this length is large $R_L = \frac{U}{\lambda\eta} >> 1$. The feedback mechanism of this α^2 dynamo is readily seen. Smallscale vortical motions produce a net electromotive force yielding a current parallel to the mean field. The largescale current in turn amplifies the mean magnetic field.

3.4 Chapter summary

At low values of the local (smallscale) magnetic Reynolds number, any externally applied magnetic fields will be slightly perturbed. The perturbed field reaches an equilibrium configuration in a time on the order of the diffusive timescale of the fluid. Though the α effect so generated is weak, it is however sufficient to destabilise magnetic fields of lengthscale $\sim O(R_m^{-2}l$. Thus a dynamo acting at the larger scale is possible. However as the mean-field evolves on a convective time larger than the local diffusive time (by a factor of R_m^{-3}), its growth is relatively slow. The large scale magnetic Reynolds number is large ($O(R_m^{-1})$) so there is no contradiction here that dynamo action occurs only when advection overcomes diffusion.

There are implications here for modelling planetary dynamos. Within the fluid cores of such bodies, small scale convective motions, even weak ones, can amplify the largescale magnetic field provided the scale length separation is sufficient, i.e., at least $O(R_m^{-2})$. Rotation favors the establishment of such vortices via the Coriolis force acting on rising convecting masses. This allows for an α^2 dynamo mechanism which could operate within planetary cores.

Chapter 4

DYNAMICAL BEHAVIOR AT LARGE R_m IN THE MODEL FLOW

4.1 Overview of the chapter

In this chapter, Roberts's cellular flow is considered at large magnetic Reynolds number. First, previous work is noted. Soward's (1987) α effect calculation is employed to write the scalarized mean field induction equation. Next the scheme for scalarization of the Navier-Stokes equation is presented. Boundary layer analysis allows the determination of the axial magnetic field and vector potential. Once determined these quantities permit calculation of magnetic force and torque terms in the (now) scalar Navier-Stokes equations. A dynamo model incorporating Lorentz back-reaction onto the fluid is thus developed via a set of three ordinary differential equations detailing the evolution of the mean magnetic field, axial and planar velocity amplitudes.

4.2 Previous results

4.2.1 Boundary layer analysis

When the magnetic Reynolds number $R_m = \frac{UL}{\eta}$ is much greater than unity, the induction equation takes the dimensionless form (Childress, 1988)

$$\frac{\partial \vec{b}}{\partial t} = \nabla \times (\vec{u} \times \vec{b}) + R_m^{-1} \nabla^2 \vec{b}. \tag{4.1}$$

The highest order term is now multiplied by a small parameter implying the existence of boundary layers needed to satisfy boundary conditions (Neyfeh, 1985). Within the boundary layer, magnetic diffusion is of the same magnitude as advection. For the present model, this layer is $O(R_m^{-1/2} L)$ where L is the cell wall length as seen by assuming $\frac{ub}{L} \sim \frac{\eta b}{l^2}$ (Childress, 1988).

Soward (1987) modified the Roberts cell flow by imposing a weak singularity in the axial vorticity at the stagnation points to produce a 'semi-fast' kinematic dynamo. However this added feature doesn't alter the α effect calculation (Perkins and Zweibel, 1987). He then determined the α effect by reducing the induction problem to a diffusion equation via transformation to Von Mises coordinates $d\sigma = |\vec{u_H}| ds$, $\xi = R_m^{1/2} \psi$ where s is the length along the separatrix $\psi = 0$. The boundary conditions were then incorporated into the solution by the Wiener-Hopf technique. He found the averaged electromotive force is found to be

$$< \vec{u} \times \vec{b} > = \alpha \vec{b_0}, \tag{4.2}$$

$$\alpha = -0.533 \frac{K}{\sqrt{R_m}} \begin{pmatrix} 1 & 0 \\ 0 & 1 \end{pmatrix}. \tag{4.3}$$

Soward also determined, using asymptotic methods, the mean field growth rate to be maximal when the axial wavenumber $\lambda \sim O(\ln R_m)$ relative to the cell length, which is consistent with the assumption of wide scale separation. Other authors (Childress, 1979; Anufriyev and Fishman, 1984; Perkins and Zweibel, 1987) have

also calculated the α effect for Roberts' cellular dynamo however Soward's analysis appears to lead to the correct asymptotic limit of the magnetic growth rate (Childress, private communication).

4.3 Formulation of the mean field induction equation

The first equation to be developed in this model is a scalar form of the mean field induction equation. Several points however should be noted. As an average of the magnetic field over many cells, the mean field $\vec{b_0}$ is independent of the planar coordinates x, y. Hence it is a vector-valued function of time and the axial coordinate z. Also, the mean field obeys the soleniodal constraint, i.e., Gauss' law, implying the axial component of $\vec{b_0}$ is at most a constant. One may set $b_{0z} = 0$ without altering the physical content of the problem. Therefore the mean field lies in the $x-y$ plane.

I assume the mean field to be of the form

$$\vec{b_0} = (b_{0x}(t)\hat{x} + b_{0y}(t)\hat{y})e^{i\lambda z} \tag{4.4}$$

where the axial wavenumber $\lambda << L^{-1}$, L being the cell wall length. Using the expression for the α effect the induction equation is written as

$$\frac{\partial \vec{b_0}}{\partial t} = i\lambda\alpha\hat{z} \times \vec{b_0} - \eta\lambda^2\vec{b_0}. \tag{4.5}$$

At this point the vector equation is transformed into a scalar one by setting $B_c = b_{0x} + i\, b_{0y}$ so that

$$\frac{dB_c}{dt} + \eta\lambda^2 B_c = -\alpha\lambda B_c. \tag{4.6}$$

The axial wavenumber λ exceeds L^{-1} by a factor of $\ln R_m$ (Soward, 1987) while α determines the α effect magnitude. Using Soward's result,

$$\alpha = -0.533V\sqrt{\frac{\eta}{LU}}. \tag{4.7}$$

Note that α has dimensions of a velocity as it should. This scalarized induction equation constitutes the first model equation.

In seeking a dynamical model incorporating the Lorentz force it is necessary to make the velocity amplitudes time-dependent i.e., $U \rightarrow U(t)$, $V \rightarrow V(t)$ to allow sufficient degrees of freedom in the equations. If the timescale of the system (i.e., $U(t)$, $V(t)$, $\vec{b}_0(t)$) is long compared to the eddy turnover time L/U, one can employ the instantaneous α effect computed from the steady cellular flow case. Likewise the magnetic force and torque exerted on the fluid is calculated using instantaneous $\vec{b}$ values. The model is based on this assumption. In that case the α effect above becomes $-0.533V(t)\sqrt{\frac{\eta}{U(t)L}}$.

4.4 The Axial momentum equation

The model second equation considers the global axial (i.e., z-direction) momentum balance. Derivation of the evolution equation for the axial velocity amplitude $V(t)$ is the goal. The eulerian z-velocity is given by $w = V(t)\sin\frac{\pi x}{L}\sin\frac{\pi y}{L}$. It is assumed this form is maintained even in the presence of Lorentz stresses. Calculation of quantities are made over the cellular region $M = (x,y,z) \mid 0 \leq x,y \leq L,\ -\infty < z < \infty)$. The fluid density ρ is assumed constant. Here I am integrating the z-component of the Navier-Stokes equation over a cell, that is

$$\rho\int_0^L\int_0^L(\frac{\partial w}{\partial t} + \vec{u}\cdot\nabla w)dxdy = \int_0^L\int_0^L(-\frac{\partial P}{\partial z} + \rho\nu\nabla^2 w + \{\vec{j}\times\vec{b}\}_z)dxdy. \quad (4.8)$$

Consider the left-hand side of equation 4.8.. The rate of change of axial momentum per unit axial length is given by

$$\frac{dm_z}{dt} = \rho\int_0^L\int_0^L\frac{\partial w(x,y,t)}{\partial t}dxdy = \frac{4L^2\rho}{\pi^2}\frac{dV(t)}{dt}. \quad (4.9)$$

Next the advective term does not contribute to the formula, i.e.,

$$\int_0^L\int_0^L \vec{u}\cdot\nabla w(x,y,t)dxdy = 0. \quad (4.10)$$

Now consider the right-hand of the integrated Navier-Stokes equation. First, the pressure gradient term yields

$$-\int_0^L \int_0^L \frac{\partial P}{\partial z} dxdy \;=\; -\frac{\partial P(\vec{c})}{\partial z} L^2 \tag{4.11}$$

for at least one $\vec{c} \in M$ by the mean-value theorem. Set $\frac{\partial P(\vec{c})}{\partial z} = -\frac{4\rho}{\pi^2}\Gamma$ so that

$$-\int\int_M \frac{\partial P}{\partial z} dxdy \;=\; \frac{4\rho L^2}{\pi^2}\Gamma. \tag{4.12}$$

This choice gives Γ units of acceleration, the same as $\frac{dV}{dt}$.

Next evaluate viscous stresses. The drag force per length in the cellular region is easily calculated and found to be

$$f_{visc} = \rho\nu \int\int_M (\frac{\partial^2}{\partial x^2} + \frac{\partial^2}{\partial y^2}) w(x,y,t) dxdy \;=\; -8\rho\nu V(t), \tag{4.13}$$

whereν is the kinematic viscosity.

The final term to evaluate is the Lorentz force per length. As with the α effect calculation, assume a uniform field $\vec{b}_0$ is maintained exterior to the cell. After flux expulsion, the steady field within the cell has the form $\vec{b} = (\frac{\partial A}{\partial y}, -\frac{\partial A}{\partial x}, B)$ due to the flow symmetry. The magnetic force per length then equals

$$f_{mag} = \mu^{-1} \int\int_M (\frac{\partial A}{\partial y}\frac{\partial B}{\partial x} - \frac{\partial A}{\partial x}\frac{\partial B}{\partial y}) dxdy, \tag{4.14}$$

where μ is the magnetic permeability. The functions A, B satisfy the relations

$$\vec{u}_H \cdot \nabla A \;=\; \eta \nabla^2 A, \tag{4.15}$$

$$\vec{u}_H \cdot \nabla B \;=\; \eta \nabla^2 B - \frac{dw}{dt}\vec{u}_H \cdot \nabla A \tag{4.16}$$

from the induction equation.

As the field is confined to a layer of thickness $O(R_m^{-1/2}L)$ it is expedient to rewrite the above formulae in the Von Mises boundary layer coordinates $\sigma = \int u_H ds$, $\hat{\psi} = R_m^{1/2}\psi$. The function A then is a solution of the one-dimensional heat equation $\frac{\partial A}{\partial \sigma} =$

$\eta\frac{\partial^2 A}{\partial\hat{\psi}^2}$ while a solution for B that satisfies the condition $B=0$ at $\psi=0$ is $\frac{1}{2}\frac{dw(0)}{d\hat{\psi}}\hat{\psi}\frac{\partial A}{\partial\hat{\psi}}$. One obtains for the Lorentz force per length

$$\begin{aligned} f_{mag} &= \mu^{-1}\int\int(\frac{\partial A}{\partial\hat{\psi}}\frac{\partial B}{\partial\sigma}-\frac{\partial A}{\partial\sigma}\frac{\partial B}{\partial\hat{\psi}})d\sigma d\hat{\psi} \qquad (4.17)\\ &= \mu^{-1}\int\int\frac{\partial}{\partial\hat{\psi}}(A\frac{\partial B}{\partial\sigma})-\frac{\partial}{\partial\sigma}(A\frac{\partial B}{\partial\hat{\psi}})d\sigma d\hat{\psi}\\ &= \int A\frac{\partial B}{\partial\hat{\psi}}d\hat{\psi}\propto\frac{V}{U}. \end{aligned}$$

The magnetic force per length can now be wriiten as $f_{mag}=-\gamma\frac{V}{U}B_cB_c^*$ where, recall, B_c is a complex number, $B_c=B_x+iB_y$, formed from the mean magnetic field and γ is a constant arising form the integrals. To verify this form of the magnetic force, note that it is expressible as a quadratic functional in B_c, $f_{mag}=\sum f_{ij}B_iB_j$ with $f_{11}=f_{22}$, $f_{12}=f_{21}$ by symmetry. But $B=1+i$ yields the same force as $1-i$ so $f_{12}=0$. Again by the symmetry of the flow we must also have $f_{11}=f_{22}$ so the force is proportional to $|B_c|^2$ as stated.

I now have the second equation of the model:

$$\frac{dV}{dt}=\Gamma-\frac{2\pi^2\nu}{L^2}V-\frac{\pi^2\gamma}{4\rho L^2}\frac{VB_cB_c^*}{U}. \qquad (4.18)$$

4.5 The axial torque equation

The third model equation details the evolution of the planar velocity amplitude $U(t)$. To arrive at this expression, I consider the rate of change of axial angular momentum equation, which may be found by taking the cross product of position from the z-axis with the Navier-Stokes equation and then integrating over a cell:

$$\int_0^L\int_0^L\vec{x}\times\{\rho(\frac{\partial\vec{u}}{\partial t}+\vec{u}\cdot\nabla\vec{u})+\nabla P-\rho\nu\nabla^2\vec{u}-\vec{j}\times\vec{b}\}_z dxdy = 0. \qquad (4.19)$$

Note we posit the spatial structure of the flow to be preserved by the viscous and magnetic torques.

The rate of change of axial angular momentum is determined to be

$$\frac{dI(t)}{dt} = -\rho \int_0^L \int_0^L x\frac{\partial \psi}{\partial x} + y\frac{\partial \psi}{\partial y} dxdy, \tag{4.20}$$
$$= \frac{8\rho L^3}{\pi^2}\frac{dU(t)}{dt}.$$

Next the advective term makes no contribution as before due to the presence of terms such as $\sin\frac{2\pi x}{L}, \sin\frac{2\pi y}{L}$ in the integrand giving a zero value for the integral.

The pressure gradient term may be considered in a mechanical sense an internal rotator supplying angular momentum to the fluid to overcome viscous and magnetic torques. The equation is found to be

$$T_p = \int_0^L \int_0^L x\frac{\partial P}{\partial y} - y\frac{\partial P}{\partial x} dxdy. \tag{4.21}$$

The exact form of the pressure gradient is not specified as before since one can again employ the mean value theorem and say the term represents an averaged value of the integrand times the cell area to be called T_0.

The viscous torque expression is determined next. One has

$$T_v = -\rho\nu \int_0^L \int_0^L x\nabla^2\frac{\partial \psi}{\partial x} + y\nabla^2\frac{\partial \psi}{\partial y} dxdy \tag{4.22}$$
$$= -16\rho\nu LU(t).$$

The final term to calculate is the magnetic torque expression. It is readily verifiable that this term is given by

$$T_{mag} = -\mu_m^{-1}\hat{z} \cdot \int\int_{cell} \vec{r} \times \vec{b} \cdot \nabla\vec{b} dxdy. \tag{4.23}$$

Note here that I am evaluating the moment of the divergence of magnetic stresses as the gradient part of $\vec{j} \times \vec{b}$ is absorbed by the fluid pressure term.

Now define the symmetric tensor $T_{ij} \equiv b_i b_j$ and let ϵ_{ijk} be the usual Levi-Civita tensor. In tensor notation the magnetic torque is determined to be

$$(T_{mag})_i = -\mu_m \int_0^L \int_0^L \frac{\partial}{\partial x_j}(\epsilon_{irs} x_r T'_{sj}) dxdy, \tag{4.24}$$

$$= \mu_m \oint_{boundary} \epsilon_{irs} x_r T_{sj} n_j ds.$$

In the boundary layer approximation appropriate to the cellular flow dynamo at large magnetic Reynolds number this expression for the magnetic torque becomes

$$T_{mag} = \mu_m \oint (x b_y - y b_x)(b_x dy - b_y dx), \tag{4.25}$$

$$\approx \frac{k}{\mu_m} B_c B_c^* L^2$$

where k is an $O(1)$ constant from the boundary layer analysis and remarks used in determination of the magnetic force term (i.e., the appearance of $|B_c|^2$) likewise apply here.

The third and last equation of the model is now given by

$$\frac{dU}{dt} = \frac{\pi^2 T_0}{8\rho L^3} - \frac{2\pi^2 \nu U}{L^2} - \frac{\pi^2 k |B_c|^2}{8\mu_m \rho L}. \tag{4.26}$$

4.6 Nondimensionalization of the equations

It is assumed in this model that the local magnetic Reynolds number is large and that over the convective time of the fluid the average magnetic and velocity fields do not vary appreciably. Whence the system evolves on the longer diffusive timescale of the mean field. So I first set

$$t = t^*(\eta\lambda^2)^{-1}, \tag{4.27}$$

where t^* is now dimensionless In what follows all starred quantities are nondimensional.

The velocity amplitudes are scaled by a common factor, hence

$$U(t) = U_0 U^*(t^*), \tag{4.28}$$

$$V(t) = U_0 V^*(t^*).$$

With the above scalings the mean field induction equation becomes

$$\frac{dB^*}{dt^*} + B^* = \alpha^* \frac{V^* B^*}{\sqrt{U^*}}, \tag{4.29}$$

where $\alpha^* = 0.533\sqrt{\frac{U_0}{L\eta\lambda^2}}$ and the magnetic field has been scaled as $B = B_0 B^*$.

The equations for U^*, V^* become respectively

$$\frac{dU^*}{dt^*} + \frac{k_v \nu \pi^2}{8L^2\eta\lambda^2}U^* - \frac{T_0\pi^2}{8\rho L^2 U_0 \eta\lambda^2} + \frac{k_t \pi^2 v_A^2}{8L\eta\lambda^2 U_0}|B^*|^2 = 0, \tag{4.30}$$

$$\frac{dV^*}{dt^*} + \frac{2\pi^2\nu}{L^2\eta\lambda^2}V^* = \frac{\Gamma}{\eta\lambda^2 U_0} - \frac{k_m \pi^3 v_A^2 V*}{4LU_0\eta\lambda^2 U^*}|B^*|^2, \tag{4.31}$$

where v_A is the Alfven velocity $\frac{B_0}{\sqrt{\rho\mu}}$.

The equation for U^* s can be further simplified by setting the value of the axial wavenumber λ so that

$$U_0 = \frac{T_0\pi^2}{8\rho L^2\eta\lambda^2} \text{ and } v_A^2 = \frac{8L\eta\lambda^2 U_0}{k_t\pi^2}. \tag{4.32}$$

Then one has the final equation for U^*:

$$\frac{dU^*}{dt^*} + \mu^* U^* = 1 - |B^*|^2, \tag{4.33}$$

$$\mu^* = \frac{k_v\nu\pi^2}{8L^2\eta\lambda^2}.$$

Setting $V^{**} = \frac{\Gamma}{\eta\lambda^2 U_0}V^*$ and letting

$$\nu^* = \frac{2\pi\nu}{L\eta\lambda^2}\frac{\Gamma}{\eta\lambda^2 U_0}, \tag{4.34}$$

$$\gamma^* = \frac{k_m\pi^2 v_A^2}{4U_0\eta\lambda^2}\frac{\Gamma}{\eta\lambda^2 U_0},$$

one has the equation for V^{**} :

$$\frac{dV^{**}}{dt^*} = \nu^* V^{**} = 1 - \gamma^*\frac{V^{**}}{U^*}|B^*|^2. \tag{4.35}$$

The alteration of V^* changes the coefficient α^* in the nondimensional induction equation. Writing $\alpha^{**} = \alpha^*\frac{\Gamma}{\eta\lambda^2 U_0}$ I then have

$$\frac{dB^*}{dt^*} + B^* = \alpha^{**}\frac{V^{**}B^*}{\sqrt{U^*}}. \tag{4.36}$$

Defining $Z = |B^*|^2$ and dropping asteriskes and the dynamo model consists of three evolution equations involving a set of four free parameters $(\alpha, \gamma, \mu, \nu)$ containing physical properties such as fluid density, conductivity, viscosity, cell size and scale length of the mean magnetic field. The formulae are

$$\frac{dU}{dt} + \mu U = 1 - Z, \tag{4.37}$$

$$\frac{dV}{dt} + \nu V = 1 - \frac{\gamma V Z}{U}, \tag{4.38}$$

$$\frac{dZ}{dt} = 2(\frac{\alpha V}{\sqrt{U}} - 1)Z. \tag{4.39}$$

Analysis of the model dynamo equations comprises the topic of the next chapter.

Chapter 5

ANALYSIS OF THE DYNAMO EQUATIONS

5.1 Chapter overview

In this chapter, the stability of equilibrium solutions of the dynamo equations as well as their temporal evolution is studied. The magnetic energy behavior over ranges of parameters is emphasized.

5.2 Equilibrium solutions of the model

Setting the time derivative in the model equations equal to zero yields the equilibria of the system. Denoting those values with subscript 'e' ,one has

$$U_e = \frac{1 - Z_e}{\mu}, \tag{5.1}$$

$$V_e = \frac{1 - Z_e}{\nu - (\gamma\mu - \nu)Z_e}, \tag{5.2}$$

$$0 = (\frac{\alpha V_e}{\sqrt{U_e}} - 1)Z_e. \tag{5.3}$$

Two cases arise from the above equations; the nonmagnetic equilibrium situation ($Z_e = 0$) and the magnetic case ($Z_e \neq 0$).

5.2.1 Case of zero Z_e

For zero Z_e, the values of the velocity amplitudes are given by

$$U_e = \mu^{-1} \text{ and } V_e = \nu^{-1}. \tag{5.4}$$

5.2.2 Case of nonzero Z_e

In this case, the constraint $U_e = \alpha^2 V_e^2$ is imposed for the velocity amplitudes to be real. From this the magnetic energy term lies between zero and one (due to the required positivity of U_e):

$$0 \leq Z_e \leq 1. \tag{5.5}$$

The result is physically understandable; Z_e is a nondimensional magnetic 'energy' which should be positive.

Solving for Z_e one has a simple quadratic equation for nonzero $\kappa = \gamma\mu - \nu$

$$\kappa^2 Z_e^2 + (2\nu\kappa + \mu\alpha^2) Z_e + \nu^2 - \mu\alpha^2 = 0, \tag{5.6}$$

$$Z_e^{\pm} = \frac{\nu}{2\kappa^2}\left[-(\frac{2\gamma\mu}{\nu} + \frac{\mu\alpha^2}{\nu^2} - 2) \pm \sqrt{(\frac{2\gamma\mu}{\nu} + \frac{\mu\alpha^2}{\nu^2} - 2)^2 + \frac{4\kappa^2}{\nu^2}(\frac{\mu\alpha^2}{\nu^2} - 1)} \right], \tag{5.7}$$

while for zero κ there is one value of Z_e namely

$$Z_e = 1 - \frac{\nu^2}{\mu\alpha^2}. \tag{5.8}$$

To insure at least one positive, real Z_e it is sufficient that $\mu\alpha^2 > \nu^2$. It will be seen that this condition suffices for the zero magnetic state to be unstable i.e., for the system to exhibit dynamo action. Also, the combinations of parameters $\frac{2\gamma\mu}{\nu}$ and $\frac{\mu\alpha^2}{\nu^2}$ determine whether the Z_e values are positive or negative, purely real or complex. Figure 5.1 illustrates this dependence.

5.2.3 Some special cases

In an inviscid fluid, $\mu = \nu = 0$. The equilibrium values U, V, and Z are given by

$$U_e = \frac{\gamma^2}{\alpha^2},\ V_e = \frac{\gamma}{\alpha^2},\ Z_e = 1. \tag{5.9}$$

For $\mu = \nu = \gamma = 1$ the α value strongly determines the nature of equilibrium solutions:

$$\text{if } \alpha < 0 \ \Rightarrow\ U_e = V_e = 1,\ Z_e = 0, \tag{5.10}$$

$$\alpha > 0 \ \Rightarrow\ U_e = V_e = \alpha^{-2},\ Z_e = 1 - \alpha^{-2}. \tag{5.11}$$

This is a case where $\kappa = 0$.

Another simple case is found by setting $\gamma = 0.5, \mu = 1$, and $\nu = 2$. For this choice of parameters, *kappa* $= -1.5$. Magnetic energy equilibrium values are given by

$$Z_e \ = \ \frac{2}{9}\left[\, 6 \ - \alpha^2 \ \pm \ \sqrt{\alpha^4 - 3\alpha^2}\, \right]. \tag{5.12}$$

In this example, $Z_e^{\pm}$ are complex when $\alpha < \sqrt{3}$. For $\sqrt{3} < \alpha < 2$, both Z_e values are positive and only $Z_e^+ > 0$ when $\alpha > 2$.

5.3 Bifurcation structure of the Z_e values

From the stability diagram (Fig. 5.1) several points can be made. First, only $Z_e^+ > 0$ for $\frac{\mu\alpha^2}{\nu^2} > 1$. For lower values, finding a positive Z_e depends on the sign of $\frac{2\gamma\mu}{\nu} - 1$. Figure 5.2 illustrates the bifurcation structure of Z_e values as a function of $\frac{\mu\alpha^2}{\nu^2}$. Such bifurcation diagrams are commonly used in dynamical systems theory. Under the constraint $\frac{2\gamma\mu}{\nu} - 1 > 0$, $Z_e = 0$ for $\frac{\mu\alpha^2}{\nu^2} < 1$; if $\frac{\mu\alpha^2}{\nu^2} > 1$ a $Z_e > 0$ appears in addition to the zero solution, asymptotically approaching $Z_e = 1$ as $\frac{\mu\alpha^2}{\nu^2} \to \infty$. This is the supercritical branch of solutions in current terminology. The subcritical branch details Z_e values for $\frac{2\gamma\mu}{\nu} - 1 < 0$. Here, $Z_e = 0$ for $\frac{\mu\alpha^2}{\nu^2}$ less than some minimum value. When $(\frac{\mu\alpha^2}{\nu^2})_{min} < \frac{\mu\alpha^2}{\nu^2}) < 1$, two additional values $Z_e^{\pm}$ appear ; beyond $\frac{\mu\alpha^2}{\nu^2} = 1$, only Z_e^+ and the zero solution remain. The subcritical branch is further divided into lower and

upper parts depending on the stability of solutions. In the next section the stability of the equilibria is studied.

5.4 Stabilty of the equilibria

In this section, small departures from equilibrium are studied using linear stability analysis. Writing $U = U_e + U_1$, $V = V_e + V_1$, and $Z = Z_e + Z_1$ and keeping only linear terms in U_1, V_1, Z_1 the equations become

$$\frac{dU_1}{dt} + \mu U_1 = -Z_1, \tag{5.13}$$

$$\frac{dV_1}{dt} + \nu V_1 = -\gamma\left(\frac{V_1 Z_e + V_e Z_1}{U_e} - \frac{U_1 V_e Z_e}{U_e^2}\right), \tag{5.14}$$

$$\frac{dZ_1}{dt} + 2Z_1 = 2\alpha\left(\frac{V_e Z_1 + V_1 Z_e}{U_e^{1/2}} - \frac{U_1 V_e Z_e}{2U_e^{3/2}}\right). \tag{5.15}$$

Consider the case $Z_e = 0$, $U_e = 1/\mu$, $V_e = 1/\nu$ solving for the perturbations yields

$$U_1(t) = U_1(0)e^{-\mu t} - \frac{Z_1(0)}{\beta + \mu}[e^{\beta t} - e^{-\mu t}], \tag{5.16}$$

$$V_1(t) = V_1(0)e^{-\nu t} - \frac{\gamma\mu Z_1(0)}{\beta\nu + \nu^2}[e^{\beta t} - e^{-\nu t}], \tag{5.17}$$

$$Z_1(t) = Z_1(0)e^{\beta t} \text{ where } \beta = 2(\frac{\alpha\sqrt{\mu}}{\nu} - 1). \tag{5.18}$$

As seen, the zero magnetic equilibrium is unstable for $\beta > 0 \rightarrow \alpha\sqrt{\mu}/\nu > 1$; any perturbation Z_1 grows exponentially away from zero. On the bifurcation diagram, the Z_e branch is stable for $\frac{\mu\alpha^2}{\nu^2} < 1$ and unstable otherwise.

Seeking solutions to equations 5.13-5.15 of the form e^{pt} leads to an eigenvalue problem. The growth rates are found from the cubic equation

$$p^3 + (\mu + \nu + \Gamma)p^2 + [\mu(\nu + \Gamma) + 2\gamma\theta - \theta]p + 2\gamma\theta\mu + \theta\Gamma - \nu\theta = 0, \tag{5.19}$$

where $\Gamma = \frac{\gamma Z_e}{U_e}$ and $\theta = \frac{\alpha V_e Z_e}{U_e^{3/2}}$.

From the above expression, determining the stability of equilibria in general is rather involved.

5.5 Numerical integration of the model equations

Using a three-dimensional numerical integration routine, equations 4.38-4.39 can be solved iteratively. I employed a fourth Runge-Kutta method in which errors are of order $O(\delta t^5)$ where δt is the timestep increment.

5.5.1 Case of $2\gamma\mu > \nu$

From the stability and bifurcation diagrams (Figs. 5.1, 5.2), when $2\gamma\mu > \nu$ the Z_e takes on the value at the supercritical branch if $\mu\alpha^2 > \nu^2$; otherwise $Z_e = 0$. Likewise, for $\mu\alpha^2 > \nu^2$, the $Z_e = 0$ branch is unstable. Figure 5.3 illustrates this. Parameters $\alpha = \gamma = 2$, $\mu = \nu = 1$ and initially $Z = 0.01$ while U and V were at their equilibrium values. The perturbation grew until reaching equilibrium at Z_e^+. Note the trajectory overshoots Z_e^+ once then converges to it. The zero branch is unstable, while the supercritical Z_e value has a large radius of attraction, meaning initially far values from it eventually spiral in. The timstep interval here is 0.003 and there are 5000 iterations corresponding to $t_{\text{final}} = 15$.

Figures 5.4 and 5.5 show the evolution of Z and U in the above example. Due to applied torques the velocity amplitude increases initially. This in turn amplifies the magnetic field. Later, the magnetic torque affects the motion causing U to begin decreasing. The magnetic field continues to increase for awhile causing the overshoot then begins to dampen due to the reduced fluid motion. Eventually, the field converges to its equilibrium value.

In Figure 5.6 the α effect is too weak to sustain the magnetic field. The field decays to zero and the velocity reaches its steady-state value $U_e = 1$.

5.5.2 Case of $2\gamma\mu < \nu$

Along the lower subcritical branch, Z_e^- is unstable; initial lower values decay to zero while initially larger values converge to the upper branch. Figures 5.7 and 5.8

illustrate this. The choice of α didn't affect the general behavior. In this range of α the zero and upper branches are attractors, while the lower branch is a repellor. No chaotic behavior was observed.

Along the upper subcritical branch, the real part of the complex growth rate becomes less negative as α increases. At some α the growth rate is purely imaginary, implying simple sinusoidal variations in time for U, V and Z. This is a Hopf bifurcation. Figure 5.9 shows V versus time. Again there is a phase lag between the velocity amplitudes and the magnetic field due to the feedback mechanism mentioned earlier.

As α increases beyond the Hopf point, the complex growth rate has a positive real part, yielding an initially growing oscillation for U, V, Z as seen in Figures 5.10, 5.11, and 5.13. Again, large magnetic energy values dampen the velocity amplitudes. Eventually the system settles onto a limit cycle, a nonlinear but regular oscillation as illustrated in Figure 5.14.

In concluding this chapter, several points should be made. First nonzero magnetic energy solutions were found; the dynamo model is successful. Along the supercritical branch the magnetic energy reaches its equilibrium, so the field is longterm stable. The subcritical branch has the more intersting behavior. As for the dynamo problem, the field will not decay along the upper branch. Oscillatory motion is achieved at and beyond the Hopf bifurcation. This latter behavior is reminiscent of secular variations in the geomagnetic field.

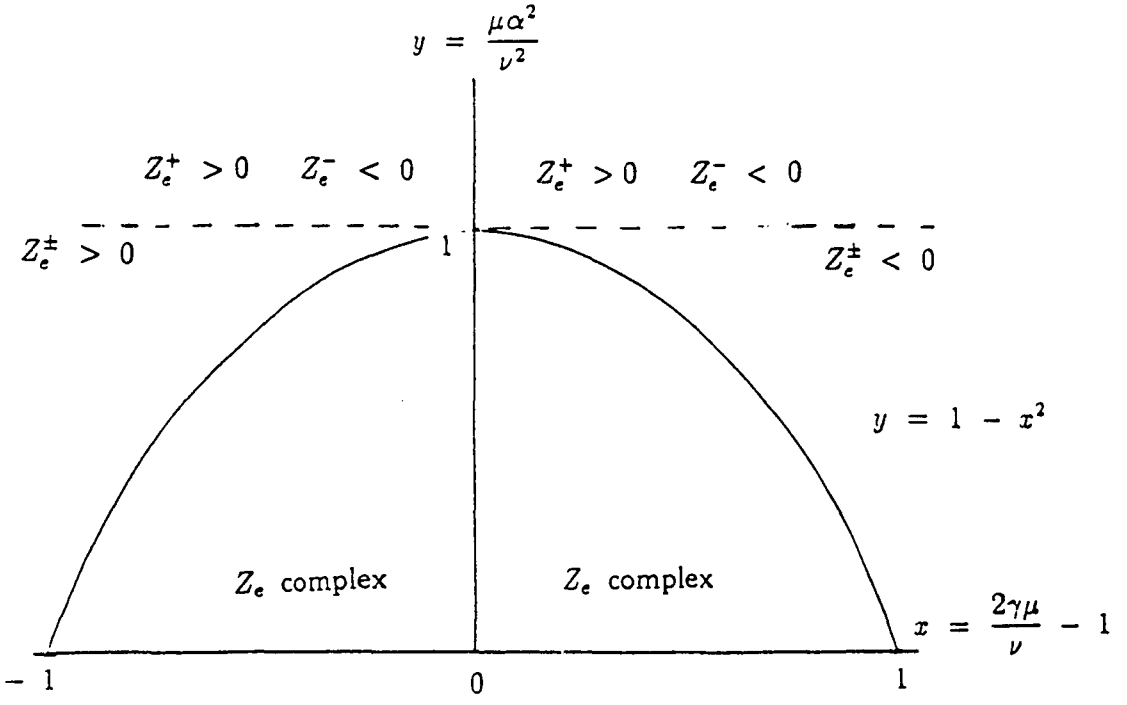

Figure 5.1: Stability diagram of Z_e

Z_e behavior is determined in the parameter space of variables $2\gamma/\nu - 1$ and $\mu\alpha^2/\nu^2$.

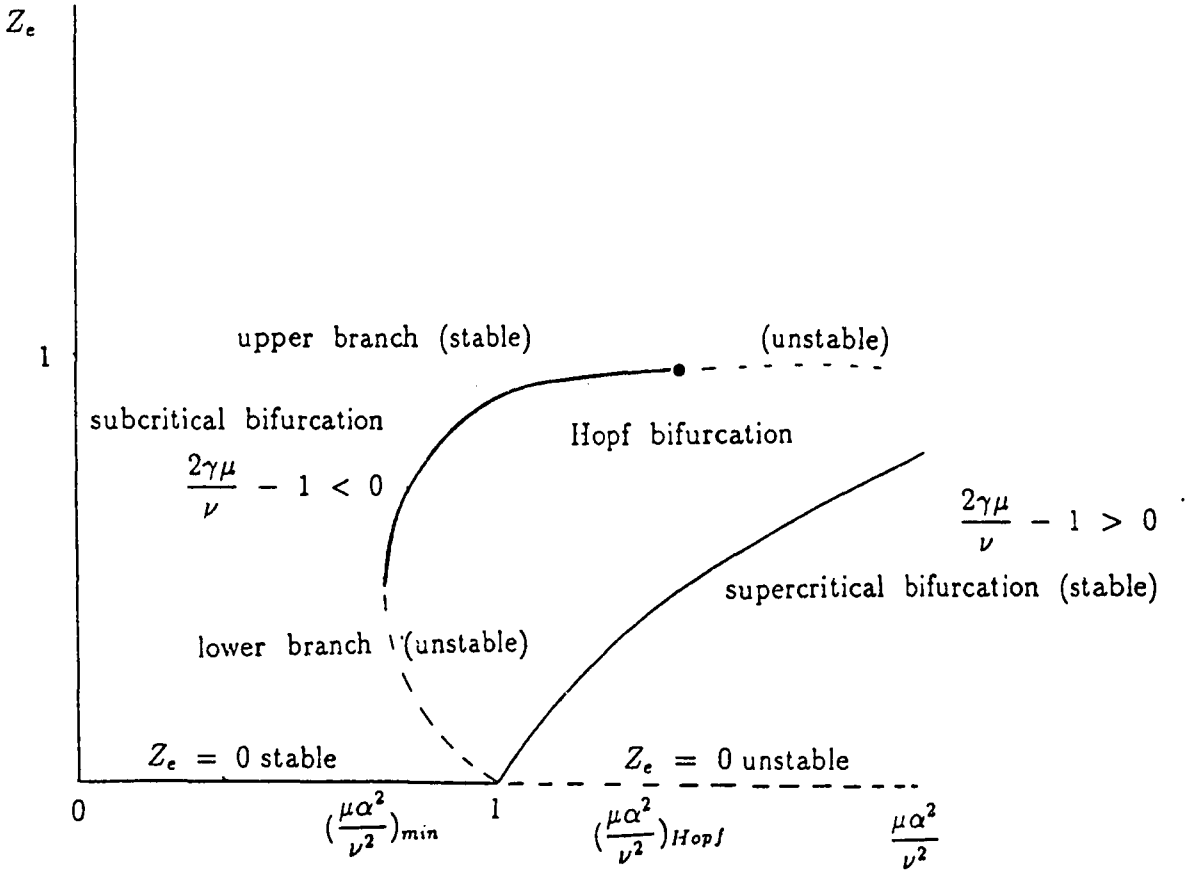

Figure 5.2: Bifurcation diagram of Z_e

Supercritical and subcritical branches correspond to nonzero Z_e. Stability of the equilibrium solutions is indicated.

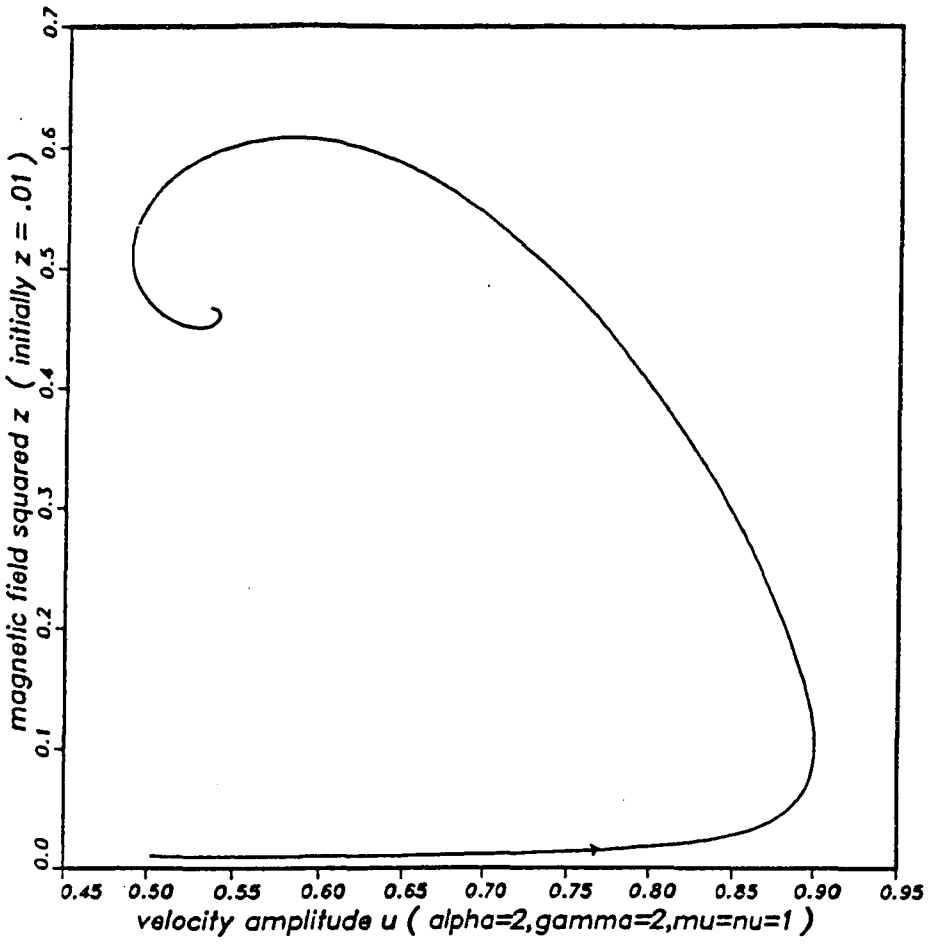

Figure 5.3: Supercritical case: phase diagram of Z vs U.

A perturbation from $Z_e = 0$ grows until equilibrium is reached at a Z_e on the supercritical branch.

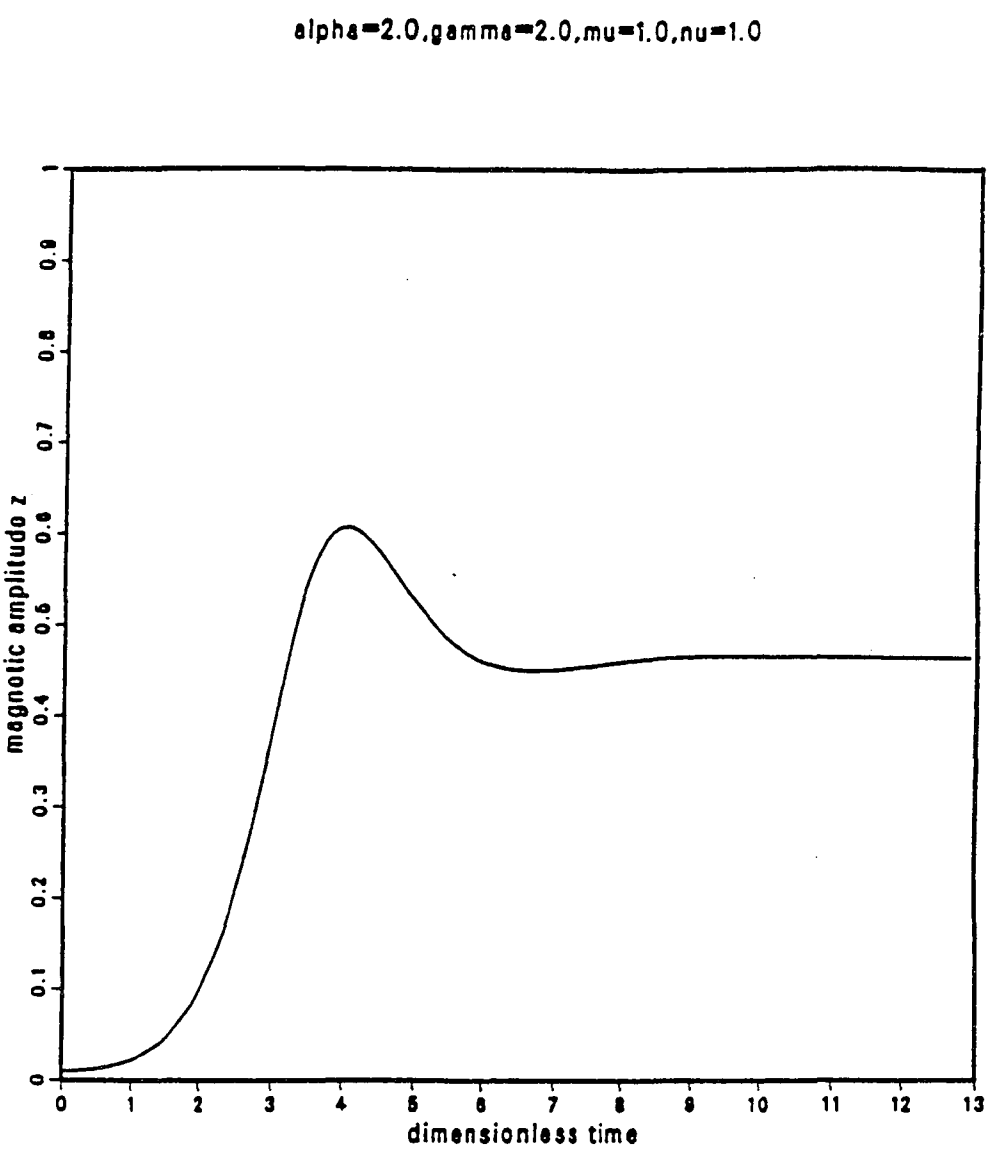

Figure 5.4: Supercritical case: Z vs t.

Z grows initially reaching maximum at $t \approx 4$ before equilibrating.

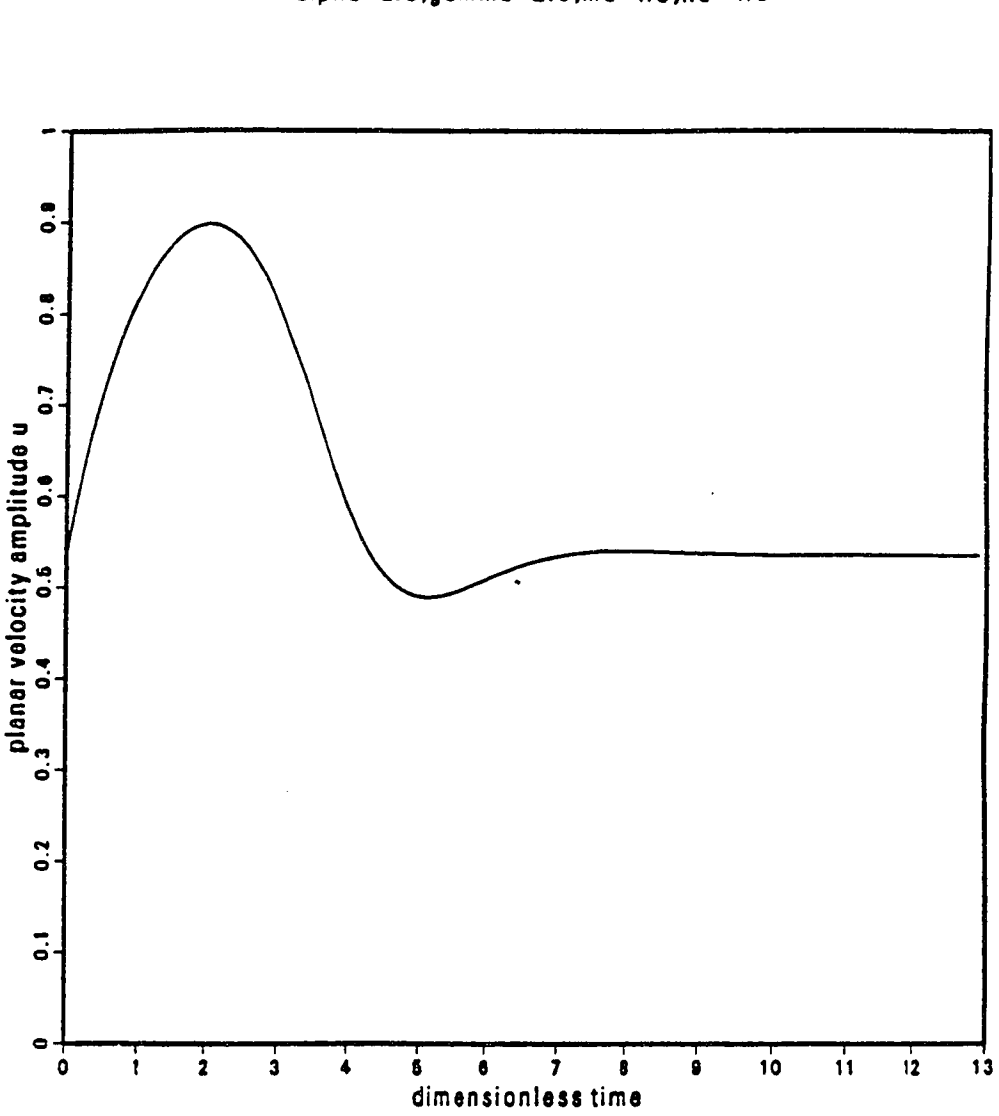

Figure 5.5: Supercritical case: U vs t.

U peaks at $t \approx 2$ before reaching equilibrium.

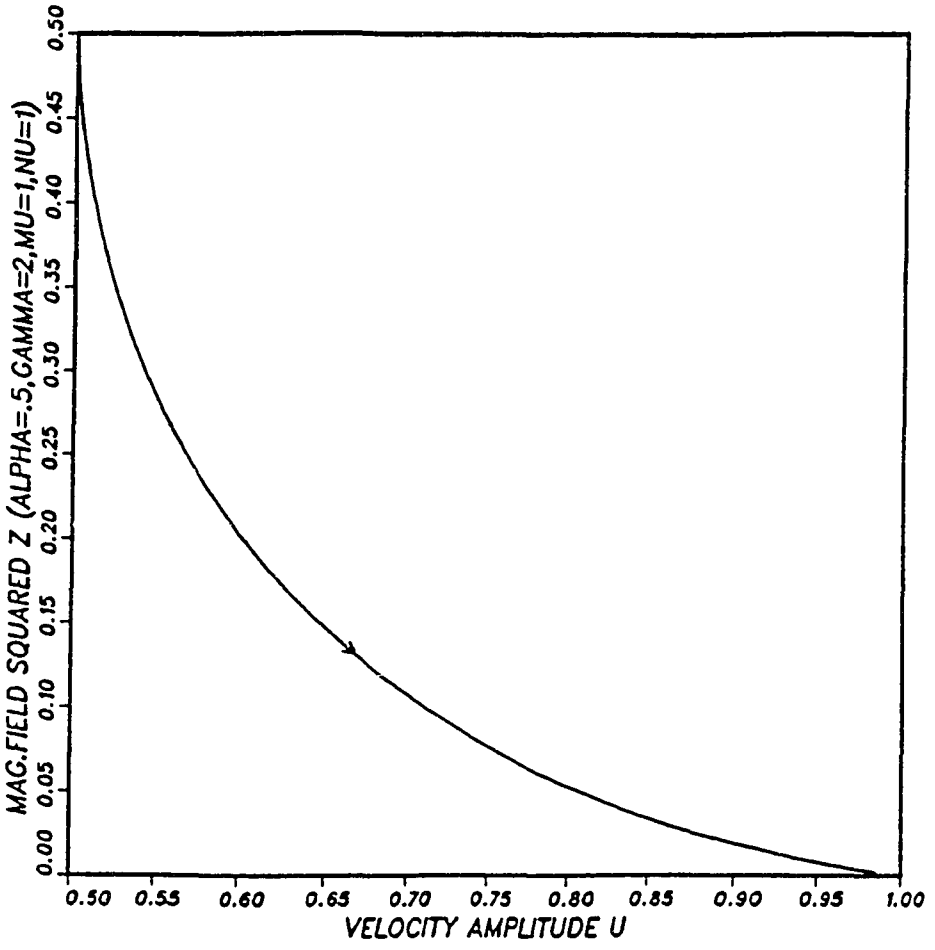

Figure 5.6: A decaying field.

Parameters correspond to negative Z_e region of stability diagram.

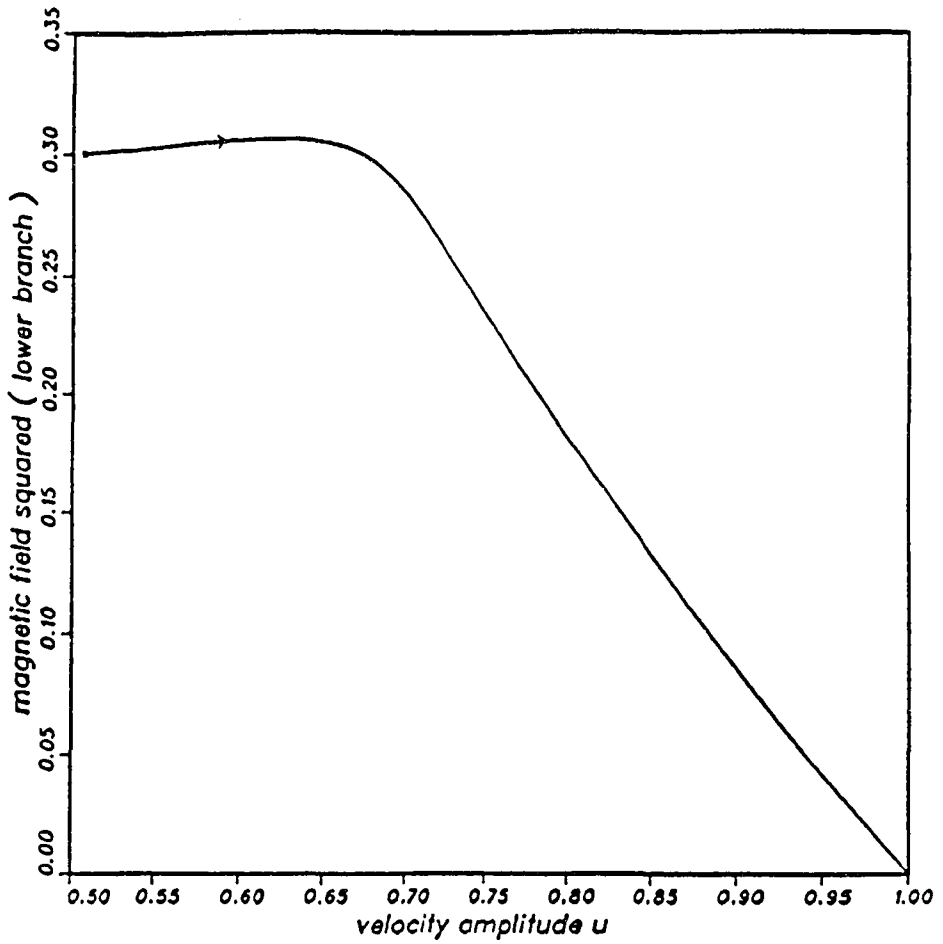

Figure 5.7: Subcritical lower branch: a field decay

Z decays when $Z(t=0) < Z_e^-$.

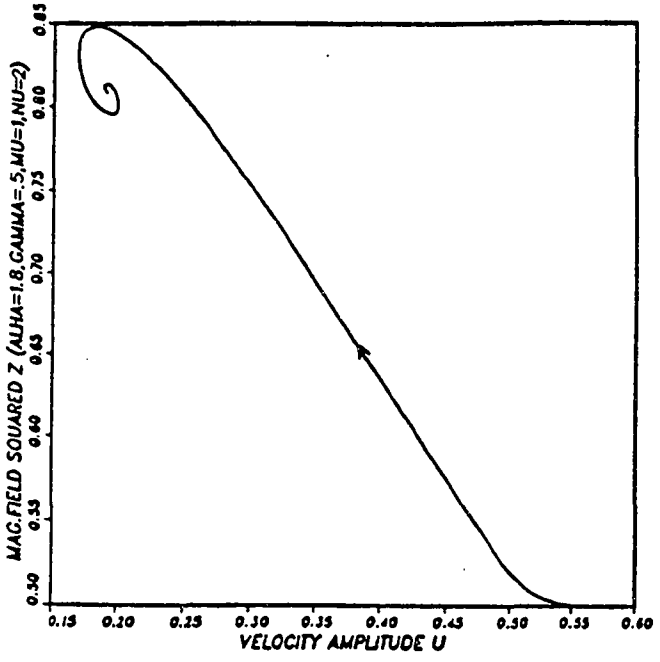

Figure 5.8: Subcritical branch: stability of upper branch.

Z increases to Z_e^+ when $Z(0) > Z_e^-$.

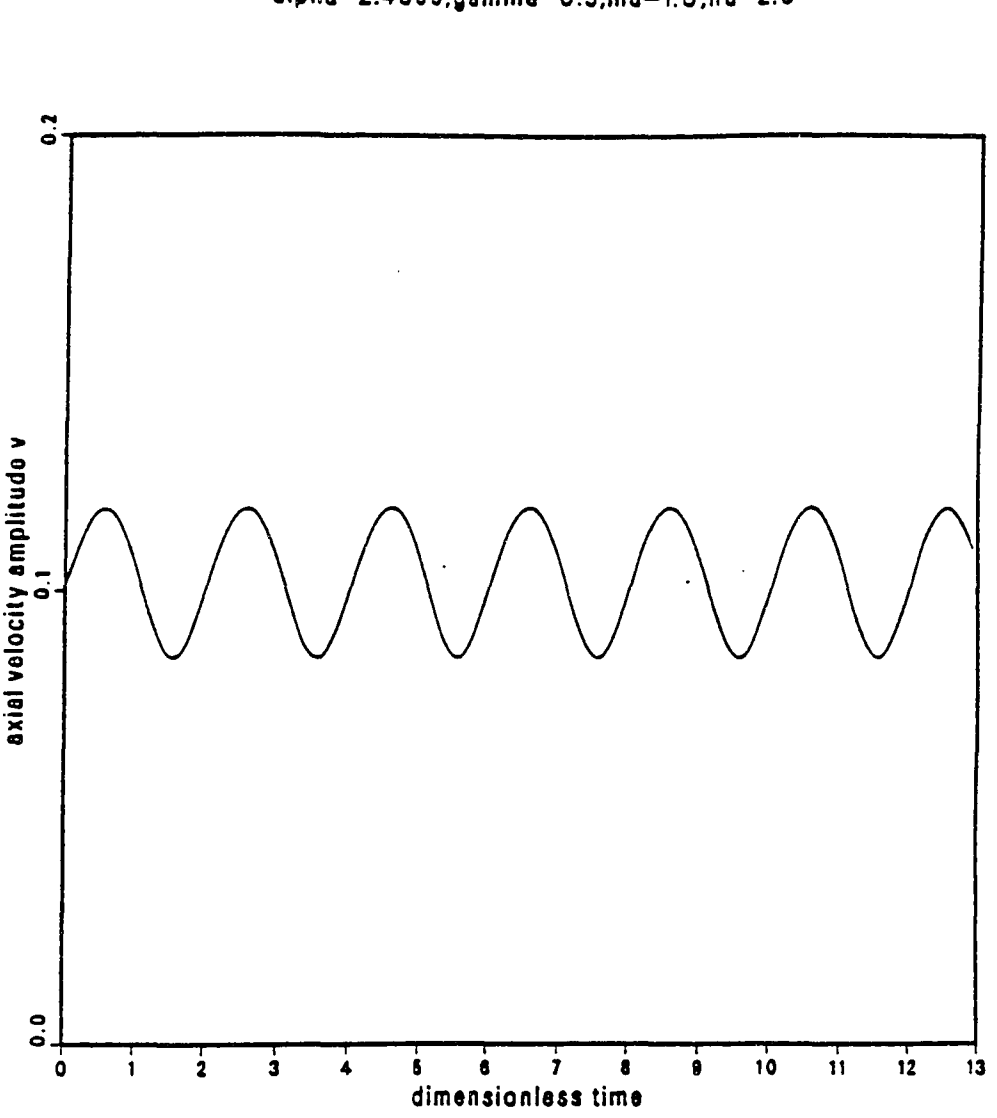

Figure 5.9: Hopf bifurcation: V vs t.

At Hopf bifurcation, U, V, Z oscillate sinusoidally.

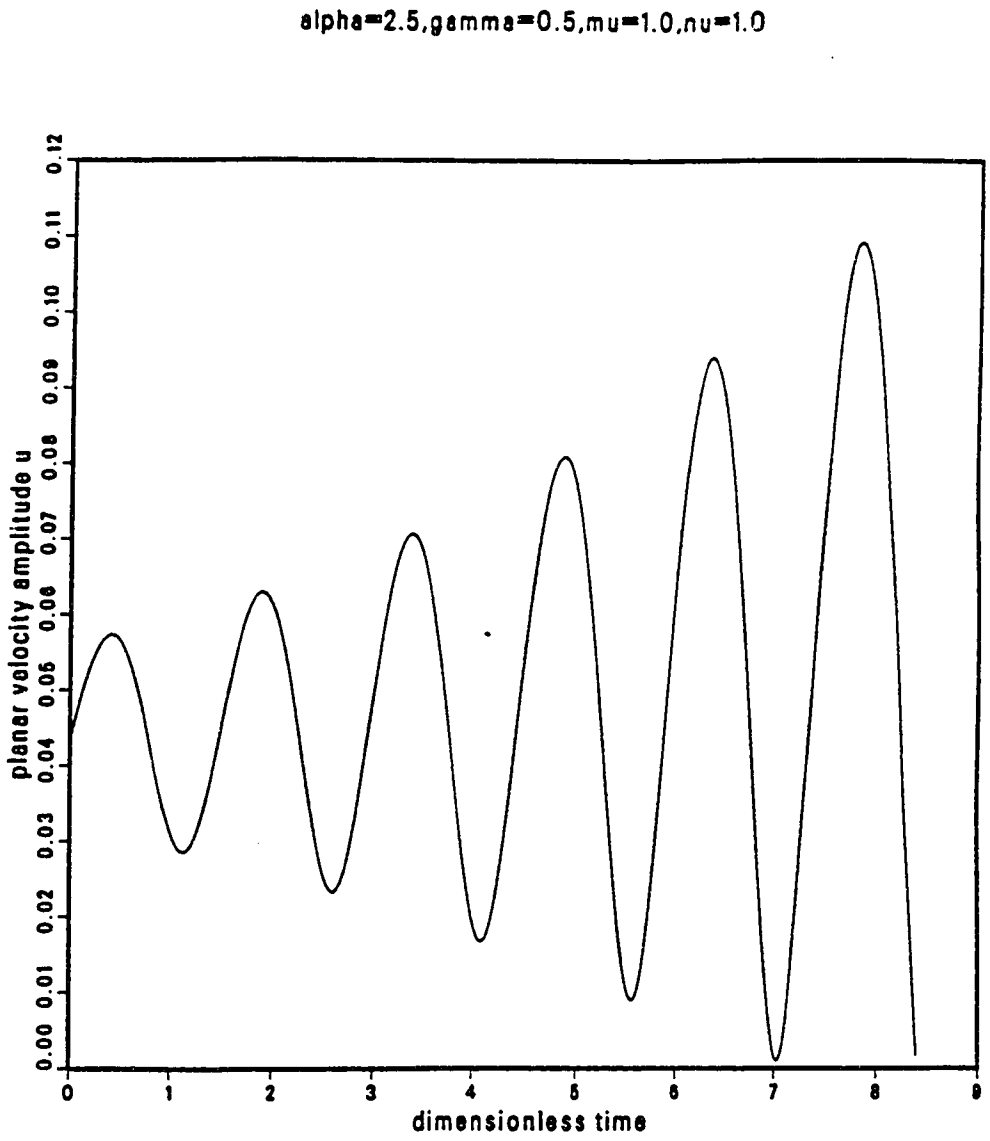

Figure 5.10: Post-Hopf: U vs t.

Beyond Hopf bifurcation, U, V, Z exhibit growing oscillations.

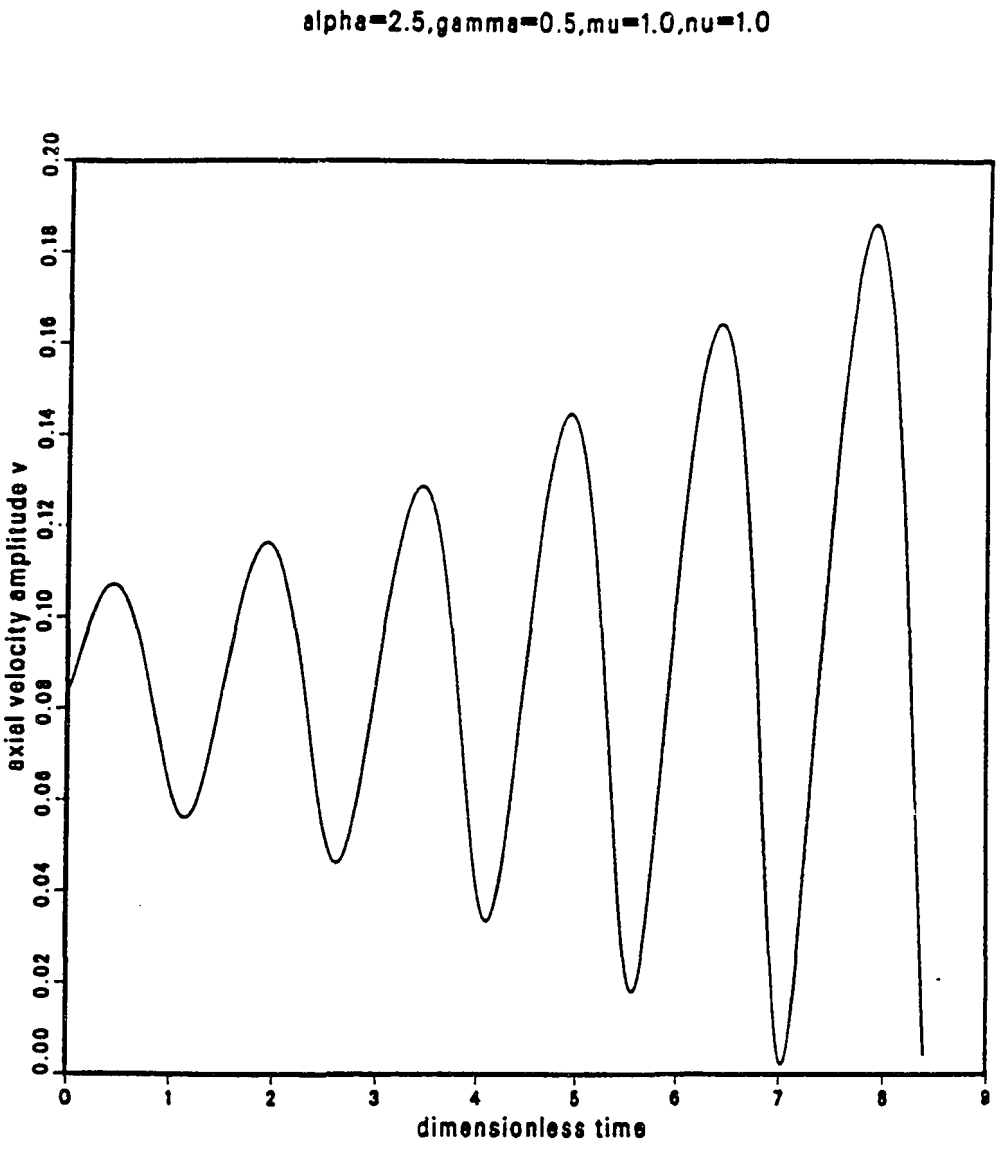

Figure 5.11: Post Hopf: V vs t.

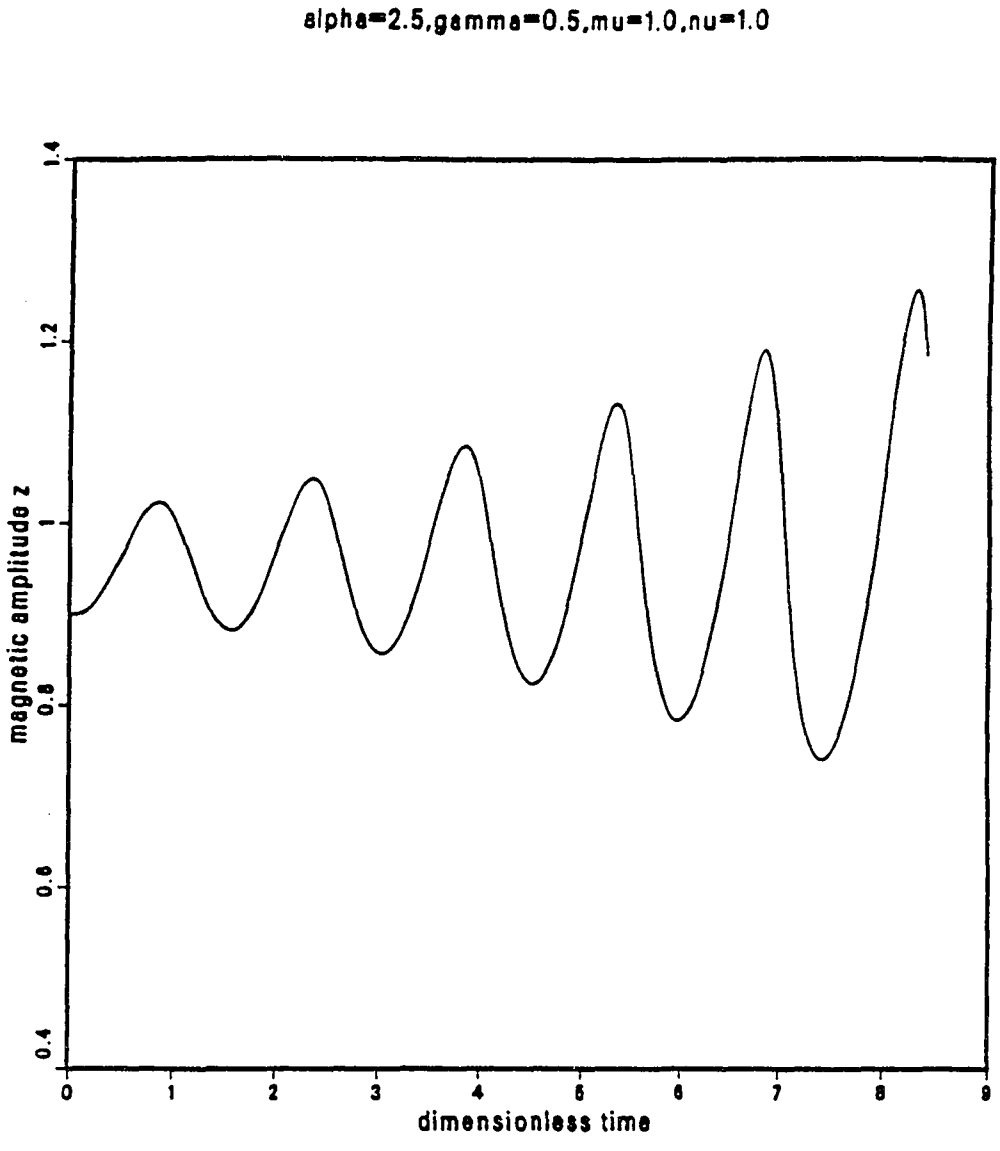

Figure 5.12: Post Hopf: Z vs t.

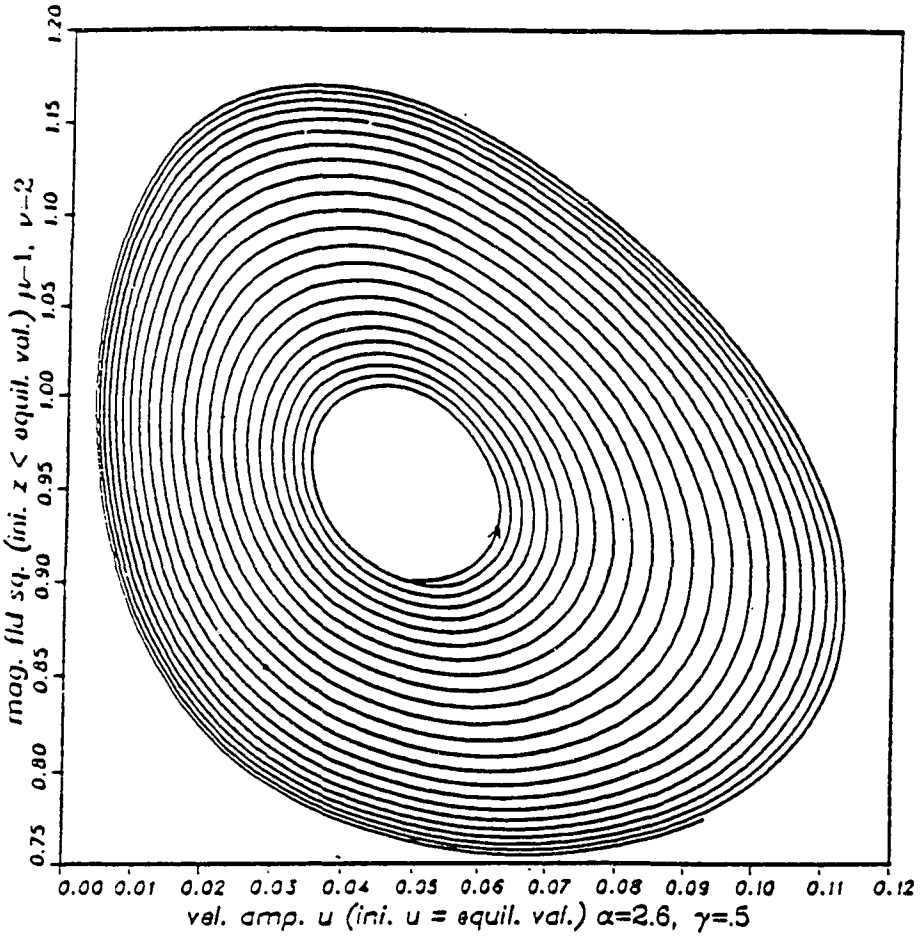

Figure 5.13: Post Hopf: Limit cycle.

Chapter 6

SUMMARY OF THE MODEL

6.1 Analysis of the model

6.1.1 The model within the context of a rotating fluid

In the geostrophic approximation valid for a rotating fluid at low Ekman and Rossby numbers (i.e., Coriolis forces dominate) the fluid motion is bidimensional, independent of the coordinate parallel to the rotation axis $\vec{\Omega}$ (Chandrasekhar, 1961). So the motivation for using the Roberts cell flow is to mimic in a simple way the convection patterns occuring in a rapidly rotating fluid. Thus in my model the z-axis is the rotation axis.

The main problem with the flow geometry I chose is the question of how to fit it into a spherical shape. Though the model assumes the cells to fill space, the same results would occur if I have a row of cells with insulating boundary conditions so that $\vec{b}$ is continuous across the boundaries. In a spherical context the model approximates an array of small cells (relative to the core radius) parallel to the rotation axis looking in the equatorial region.

In the experiments of Busse and Carrigan (Melchior, 1986) it was observed that convection in a rotating sphere led to the establishment of Taylor columns similar to the cellular array mentioned. In the experiment the axial velocity did depend on the z-coordinate due to constraints imposed by the boundaries.

To impose the Roberts cell model onto the geodynamo leads to the observation that the mean field represents the toroidal component of the core field. This is less effective that a description of the poloidal field observed at the surface. However that weakness is partially remedied by noting the mean toroidal current flux generated

$$< \vec{u} \times \vec{b} > = \alpha \vec{b} = \sigma^{-1} < \vec{j} > \tag{6.1}$$

would drive the poloidal field, indeeed the α effect is the by mechanism by which poloidal field is regenerated. So one can thus argue that variations in the toroidal field results in similar fluctuations in the poloidal field via the α effect. This is an ad hoc assumption but is justified by the physics.

6.2 Stability and bifurcation analysis of the model

In the previous chapter the equilibrium values of the magnetic field and velocity amplitudes were derived first. These values represent the $t \rightarrow \infty$ limits for the supercritical bifurcation branch developed from the parameter space. So the mode lequations are capable of yielding a case of stable magnetic field. It is noted that there have been periods in the geologic record where the field did not frequently reverse (e.g., the Permian and Cretaceous eras). Recently Gubbins (1994) has proposed a controversial theory that long-term field behavior is regulated by changes at the core-mantle boundary, as the timescale for the cycles of reversal frequency are comparable to mantle convection turnover time. One can infer from the model that the parameters I developed may be nonconstant when applied to the geodynamo. I could at a later time include such a time dependency. The model is capable of incorporating the Gubbins theory.

For the subcritical region in the parameter space, the field decays if it is initially below its equilibrium value and grows to a upper branch value if initially above equilibrium. On the upper branch, growing oscillations of the field were found for

values of α greater than the critical value determining the Hopf bifurcation point. Eventually the field oscillations ceased growing at the limit cycle so that a periodic behavior was developed. This behavior while not a field 'reversal' does mimic the geodynamo to some extent, the best analogy being secular variations and aborted reversal events.

For the lower part of the stability diagram where $\mu\alpha^2/\nu^2 < 1$ but not the subcritical branch, only the zero field solution is stable. The values of the parameters in this range produce no dynamo. This sets a limit on the values of viscosity and diffusivity in the early fluid core. Obviously no field would have evolved in this parameter range.

While evolving the set of equations numerically I observed that there is a lag time between the velocity and the magnetic field. This is a consequence of the negative feedback the magnetic field imposes on the velocity. On the supercitical branch the velocity and field would initially growth with the velocity graph (versus time) having a negative curvature. The velocity would peak first, then begin to decay. For a while the magnetic field would continue to grow in a form of an overshoot; after the velocity had declined then the field would begin to damp. Then the field would grow slightly again, evolving toward its steady-state value. This feedback is illustrated in Figures 5.4-5.5.

6.2.1 Manetic stresses and pathlines

The goal of this research was to produce a model incorporating the Lorentz force into the fluid motion equation. I added extra degrees of freedom were to prevent over-determination of the system by making the velocity amplitudes functions of time. Fluid particles maintained the same pathlines as in the constant-amplitude case. While this restriction simplified the physics, since pathlines and streamlines do not generally coincide in time-dependent flows, the requirement that the streamlines remain unaltered is unphysical. Maxwell stresses will deform a flux tube because the

hydrostatic pressure will not generally balance the magnetic pressure (an exception being the 'force-free' case where current flux is parallel to the magnetic field). However the model does have the advantage of remaining tractable. Moreover the purely kinematic dynamo models always assume fixed streamlines, the typical justification being that the kinematic case is valid when the field is weak (i.e., when the Maxwell stress is less than, the Reynolds stress). Thus the present model is best described as a 'semi-dynamical' approach with an inherent weak-field structure and represents an improvement over kinematic dynamos.

In my model the velocity is continuous across cell boundaries, unlike those models requiring large or infinite shear to form a strong omega effect such as the Ponomarenko dynamo (cf. Zeldovich et al., 1983; Gilbert, 1988) or the various disc dynamo models. This feature eases the jump conditions as the magnetic field and current flux will be continuous across boundaries.

6.3 Future Directions

In this dissertation, Roberts cellular flow has been developed into a model dynamo illustrating feedback between the magnetic and velocity fields. One may expand upon this work in several ways. More efficient dynamo generation may be produced by altering the flow by the addition of non-integrable terms in the velocity field. This would have the effect of making the flow 'chaotic'; in regions near the separatrices $\psi = 0$ fluid particles would tend to separate exponentially in time in a so-called stochastic web. Also I would consider other similar flows but in cylindrical or spherical coordinates. Cellular structures would arise from the stream function. Another avenue of useful pursuit would be to maintain the present model but allow the four parameters α, γ, μ, and ν to vary in time sinusoidally.

References

Anufriyev, A.P. & Fishman, V.M. 1982 Magnetic field structure in the two-dimensional motion of a conducting fluid. *Geomag. Aeron.* **22**, 245-248.

Barton, G. 1989 *Elements of Green's Functions and Propagation.* Clarendon Press, Oxford.

Bullard, E.C. 1955 The stability of a homopolar dynamo. *Proc. Camb. Phil. Soc.* **51**, 744-760.

Bullard, E. C. & Gellman, H. 1954 Homogeneous dynamos and terrestrial magnetism. *Phil. Trans. Roy. Soc.* **A247**, 213-278.

Busse, F. H. & Wicht, J. 1992 A simple dynamo caused by conductivity variations. *Geophys. Astrophys. Fluid Dynam.* **64**, 4, 193-203.

Catteneo, F. 1988 Low order model of the solar dynamo. *Woods Hole Oceanographic Inst. Tech. Rep.* WHOI 88-16.

Chandrasekhar, S. 1961 *Hydrodynamic and Hydromagnetic Stability.* Clarendon Press, Oxford.

Childress, S. 1978 Dynamo mdels of geomagnetism. *Woods Hole Oceanographic Inst. Tech. Rep.* WHOI 78-67.

Childress, S. 1979 Alpha-effect in flux ropes and sheets. *Phys. Earth Planet. Int.* **20**, 172-180.

Childress, S. 1988 Order and disorder in planetary dynamos. *Woods Hole Oceanographic Inst. Tech. Rep.* WHOI 88-16.

Childress, S. & Ghil, M. 1987 *Topics in Geophysical Fluid Dynamics: Atmospheric Dynamics, Dynamo Theory, and Climate Dynamics.* Springer-Verlag, New York.

Cook, A. E. & Roberts, P. H. 1970 The Rikitake two-disc dynamo system.*Proc. Camb. Phil. Soc.* **68**, 547-69.

Cox, A. 1969 The lengths of geomagnetic polarity intervals. *J. Geophys. Res.* **73**, 3247-3260.

Falicov, L. M. 1966 *Group Theory and Its Applications.* University of Chicago Press.

Fearn, D. R. & Proctor, M. R. E. 1984 Self-consistent dynamo models driven by hydromagnetic instabilities. *Phys. Earth Planet. Int.* **36**, 78-84.

Fearn, D. R. & Proctor, M. R. E. 1986b Self-consistent hydromagnetic dynamos. *Geophys. Astrophys. Fluid Dynam.* **38**, 4, 293-326.

Gilbert, A.D. 1988 Fast dynamo action in the Ponomarenko dynamo *Geophys. Astrophys. Fluid Dynam.* **44**, 241-258.

Gilbert, A. D., Frisch, U., & Pouquet, A. Helicity is unnecessary for alpha effect dynamos, but it helps. *Geophys. Astrophys. Fluid Dynam.* **42**, 151-161.

Gilman, P. A. 1983 Dynamically consistent nonlinear dynamos driven by convection in a rotating spherical shell. II. Dynamos with cycles andstrong feedbacks. *Astrophys. J. Supp.* **53**, 243-268.

Gilman, P. A. & Miller, J. 1981 Dynamically consistent nonlinear dynamos driven by convection in a rotating spherical shell. *Astrophys. J. Supp.* **46**, 211-238.

Glatzmaier, G. A. 1984 Numerical simulations of stellar convective dynamos I. The model and the method. *J. Comp. Phys.* **55**, 461-484.

Gubbins, D. 1994 Geomagnetic polarity reversals: a connection with secular variation and core-mantle interaction? *Rev. Geophys.* **32**, 1, 61-83.

Hagee, V. L. & Olson, P. 1991 Dynamo models with permanent dipole fields and secular variation *J. Geophys. Res.* **96**, B7. 11673-11687.

Jackson, J.D. *Classical Electrodynamics.* 2nd edition, John Wiley & Sons.

Krause, F. & Raedler, K.-H. 1980 *Mean-Field Magnetohydrodynamics and Dynamo Theory.* Pergamon Press.

Kropachev, E. P. 1971 Numerical solution of the equations of the dynamo theory of terrestrial magnetism. II. Results. *Geomag. Aeron.* **11**, 737-743.

Malkus, W. V. R. 1967 Hydromagnetic planetary waves. *J. Fluid Mech.* **28**, 793-802.

McMillan, J. F. 1988 A quasi-dynamical dynamo model *Woods Hole Oceanographic Inst. Tech. Rep.* WHOI 88-16.

Melchior, P. 1986 *The Physics of the Earth's Core.* Pergamon Press.

Merrill, R. T. & McElhinney, M. W. 1987 *The Earth's Magnetic Field: Its History, Origin, and Planetary Perspective.* Academic Press.

Moffatt, H. K. 1978 *Magnetic Field Generation In Electrically Conducting Fluids.* Cambridge University Press.

Parker, E. N. 1955 Hydromagnetic dynamo models. *Astrophys. J.*, **122**, 293-314.

Parker, E. N. 1979 *Cosmical Magnetic Fields.* Clarendon Press, Oxford.

Pearson, C. E. 1974 *Handbook of Applied Mathematics.* Van Nostrand-Reinhold.

Perkins, F. W. & Zweibel, E. G. 1987 A high magnetic Reynolds number dynamo. *Phys. Fluids.*, **30**, 4, 1079-1084.

Rikitake, T. 1958 Oscillations of a system of disk dynamos. *Proc. Camb. Phil. Soc.*, **54**, 89-105.

Robbins, K. A. 1977 A new approach to subcritical instability and turbulent transitions in a simple dynamo. *Proc. Camb. Phil. Soc.* **82**, 309-329.

Roberts, G. O. 1970 Spatially periodic dynamos *Phil. Trans. Roy. Soc.* **A266**, 535-558.

Roberts, G. O. 1972 Dynamo action of fluid motions with two dimensional periodicity. *Phil. Trans. Roy. Soc.* **A271**, 411-454.

Steenbeck, M., Raedler,K.-H., & Krause, F. 1966 A calculation of the mean electromotive force in an electrtically conducting fluid in turbulent motion, under the influence of Coriolis forces. *Z. Naturforsch.* **21a**, 369-376.

Smylie, D. E. & Rochester, M. G. 1981 Compressibility, core dynamics and the subseismic wave equation. *Phys. Earth Planet. Int.* **24**, 308-319.

Soward, A. M., Editor. 1983 *Stellar and Planetary Magnetism.* Gordon and Breach Publishers.

Soward, A. M. 1987 Fast dynamo action in a steady flow. *J. Fluid Mech.* **180**, 267-295.

Tritton, D. J. 1987 *Physical Fluid Dynamics.* Clarendon Press, Oxford.

Weiss, N. O. 1966 The expulsion of magnetic flux by eddies. *Proc. Roy. Soc.* **A293**, 310-328.

Zaslavsky, G. M., Sagdeev, R. Z., Usikov, D. A. & Chernikov, A. A. 1991 *Weak Chaos and Quasi-Regular Patterns.* Cambridge University Press.

Zeldovich, Ya. B., Ruzmaikin, A. A. & Sokoloff, D. D. *Magnetic fields in astrophysics.* Gordon and Breach Publishers.